Atmospheric
Chemistry
and Physics
Discussions

EGU

1 **Impacts of condensable particulate matter on atmospheric organic aerosols and fine**

2 **particulate matter (PM$_{2.5}$) in China**

3

4 Mengying Li[1], Shaocai Yu[1+], Xue Chen[1], Zhen Li[1], Yibo Zhang[1], Zhe Song[1], Weiping Liu[1], Pengfei
5 Li^{2+}, Xiaoye Zhang[1,3], Meigen Zhang[4,5,6], Yele Sun[4,5], Zirui Liu[4,5], Caiping Sun[7], Jingkun Jiang[8,9],
6 Shuxiao Wang[8], Benjamin N. Murphy [10], Kiran Alapaty[10], Rohit Mathur[10], Daniel Rosenfeld[11], and John
7 H. Seinfeld[12]

8

9 [1]Research Center for Air Pollution and Health; Key Laboratory of Environmental Remediation and
10 Ecological Health, Ministry of Education, College of Environment and Resource Sciences, Zhejiang
11 University, Hangzhou, Zhejiang 310058, P.R. China
12 [2]College of Science and Technology, Hebei Agricultural University, Baoding, Hebei 071000, P.R. China
13 [3]Chinese Academy of Meteorological Sciences, China Meteorological Administration, Beijing 100081,
14 China.
15 [4]State Key Laboratory of Atmospheric Boundary Layer Physics and Atmospheric Chemistry (LAPC),
16 Institute of Atmospheric Physics (IAP), Chinese Academy of Sciences (CAS), Beijing 100029, China
17 [5]University of Chinese Academy of Sciences, Beijing 100049, China
18 [6]Center for Excellence in Urban Atmospheric Environment, Institute of Urban Environment, Chinese
19 Academy of Sciences, Xiamen, China
20 [7]Chinese Research Academy of Environmental Sciences, Beijing 100012, China
21 [8]State Key Joint Laboratory of Environment Simulation and Pollution Control, School of Environment,
22 Tsinghua University, Beijing 100084, China
23 [9]State Environmental Protection Key Laboratory of Sources and Control of Air Pollution Complex,
24 Beijing 100084, China
25 [10]Center for Environmental Measurement and Modeling, U.S. Environmental Protection Agency,
26 Research Triangle Park, NC 27711, USA
27 [11]Institute of Earth Sciences, The Hebrew University of Jerusalem, Jerusalem, Israel
28 [12]Division of Chemistry and Chemical Engineering, California Institute of Technology, Pasadena, CA
29 91125, USA.
30
31

32 *Correspondence to*: Shaocai Yu (shaocaiyu@zju.edu.cn); Pengfei Li (lpf_zju@163.com)

33

34

35

36   **Abstract**

37   Condensable particulate matter (CPM) emitted from stationary combustion and mobile sources

38   exhibits high emissions and a large proportion of organic components. However, CPM is not generally

39   measured when conducting emission surveys of PM in most countries, including China. Consequently,

40   previous emission inventories have not included emission rates for CPM. Here we construct an emission

41   inventory of CPM in China with a focus on organic aerosols (OA) based on collected CPM emission

42   information. Results show that OA emissions are enhanced twofold after the inclusion of CPM in a new

43   China inventory for the years 2014 and 2017. Considering organic CPM emissions and model

44   representations of secondary OA (SOA) formation from CPM, here a series of sensitivity cases have been

45   simulated using the three-dimensional Community Multiscale Air Quality (CMAQ) model to estimate the

46   contributions of CPM emissions to atmospheric OA and fine PM ($PM_{2.5}$) concentrations in China.

47   Compared with observations during a haze episode from October 14 to November 14, 2014, at a Beijing

48   site, estimates of temporal average primary OA (POA) and SOA concentrations are greatly improved after

49   including the CPM effects. These scenarios demonstrated the significant contributions of CPM emissions

50   from stationary combustion and mobile sources to POA (53 ~ 86%), SOA (48 ~ 67%), and total OA

51   concentrations (50 ~ 78%). Furthermore, contributions of CPM emissions to total OA concentrations were

52   demonstrated over the major 2+26 cities of Beijing-Tianjin-Hebei region (BTH2+26 cities) in December

53   2018, with average contributions up to 55%, 58%, 60%, and 57% for Handan, Shijiazhuang, Xingtai, and

54   Dezhou, respectively. Correspondingly, the inclusion of CPM emissions also narrowed the gap between

55   simulated and observed $PM_{2.5}$ concentrations over the BTH2+26 cities. These results improve the

56   simulation performance of atmospheric OA and $PM_{2.5}$, and may provide important implications for the

57   sources of OA.

58

59

60

61

62

63

64

65

66

1 Introduction

Atmospheric fine particulate matter ($PM_{2.5}$, particulate matter with aerodynamic diameter not exceeding 2.5 μm) is a serious and recurring air quality problem. Although the annual average concentration of $PM_{2.5}$ in China has declined in recent years, it still exceeds standards promulgated by the World Health Organization (WHO) Air Quality Guidelines (Lin et al., 2018). Heavy haze episodes occur frequently in winter, especially for the eastern regions in China (Li et al., 2015; Chen et al., 2019; Li et al., 2017a). Despite large reductions in primary emissions during the COVID-19 lockdown, several periods of heavy haze continued to occur in eastern China (Huang et al., 2021; Wang et al., 2020c, 2021). Organic aerosols (OA) contribute a large fraction to the $PM_{2.5}$ worldwide, ranging from 20% to 90% (Carlton et al., 2009; Kanakidou et al., 2005) with a negative impact on radiative climate forcing, air quality and human health (Gehring et al., 2013; Pope et al., 2002). POA comes from a variety of sources, including fossil fuels and biomass burning. SOA is generated through photochemical oxidation of volatile organic compounds (VOCs) followed by gas-particle partitioning of low-volatility organic compounds into the aerosol phase (Fuzzi et al., 2006; Kroll and Seinfeld, 2008) Currently, the significant contributions of OA to $PM_{2.5}$ and SOA to OA have been demonstrated in many observational results (He et al., 2020; Veld et al., 2021; Zhang et al., 2017). For example, Huang et al. (2015) explored the role of OA in $PM_{2.5}$ during a severe haze episode in Beijing, Shanghai, Xi'an and Guangzhou, showing the substantial contribution of OA to $PM_{2.5}$ (30~50%) and SOA accounted for 30~77% of OA. Sun et al. (2015) showed that OA constituted up to 65% of submicron aerosols during winter in Beijing, with 38% being SOA.

With respect to chemical schemes of SOA formations, a two-product model (Odum et al., 1996) was first proposed based on absorptive partitioning theory (Pankow, 1994) and chamber data. To address the underestimation of the early two-product model, the volatility basis set (VBS) framework was developed (Donahue et al., 2006). In this VBS scheme, semi-volatile and intermediate volatility precursors (S/IVOCs) were classified by their volatilities based on the absorptive partitioning theory (Robinson et al., 2007). A large portion of SVOCs are emitted as POA and then evaporate at ambient conditions due to gas-particle partitioning, while the IVOCs species exist in the form of organic vapor under many atmospheric conditions in the absence of photochemical reactions (Shrivastava et al., 2011). Currently, the VBS mechanism has been incorporated into many global and regional scale models (Lane et al., 2008; Murphy and Pandis, 2009; Shrivastava et al., 2008; Han et al., 2016). The two-dimensional (2-D) VBS scheme was put forward to improve the accuracy of fragmentation processes and OA oxidations (Donahue et al., 2011; Zhao et al., 2016). Despite advances in SOA formation mechanisms, a gap exists between observed

98   and modeled results due to uncertainties in parameterization of SOA yields, inapplicability of parameter

99   localizations caused by regional and sectoral differences and incomplete information on emission rates

100   and properties of SOA precursors. Recent studies have begun to focus on important effects of emissions,

101   including traditional precursors (VOCs) and low-volatility precursors (S/IVOCs). For example, Zhao et

102   al. (2017) found that IVOC of 1.5–30 times POA emissions contributed largely to OA concentrations over

103   the BTH region. Wu et al. (2019) constructed an inventory of S/IVOCs for the Pearl River Delta (PRD)

104   region in China and conducted a simulation using the WRF-Chem model leading to an increase of 161%

105   in SOA predictions. Emissions of S/IVOCs from mobile sources and IVOCs from volatile chemical

106   products were also parameterized in models to represent SOA formation (Jathar et al., 2017; Lu et al.,

107   2020; Pennington et al., 2021). Although the significant role of potential emission sources in OA

108   formation has been demonstrated, underestimation of SOA by current air quality models has not been

109   totally resolved. Stationary combustion sources are one of the major emission sources of $PM_{2.5}$, including

110   power plants and factories. Sampling temperatures and dilution rates are key factors for accurate

111   measurements of organic matter (Morino et al., 2018). The total primary PM emitted from stationary

112   sources is composed of filterable PM (FPM) and condensable PM (CPM). FPM exists in liquid or solid

113   phases, while CPM is in gas phase in flue (Corio and Sherwell, 2000; Feng et al., 2018). CPM is defined

114   by the U.S. Environmental Protection Agency (EPA, 2017) as particles which are gaseous at flue gas

115   temperature but condense or react in the ambient air to form solid or liquid PM through dilution and

116   cooling immediately after discharge. With ultralow emission standards implemented by coal-fired power

117   plants (<10 mg/Nm^3) since 2014, FPM emissions have been substantially reduced (even below 5 mg/Nm^3)

118   (Tang et al., 2019), making the remaining emissions of CPM an important issue. The Ministry of Science

119   and Technology of China issued a national key research and development project on the causes and

120   controls of air pollution in 2016, which mentioned key technologies for controlling CPM emissions

121   (http://www.acca21.org.cn/zdy_cms/siteResources/DisasterReduction/resources/otherfiles/

122   20160425/f15345793.pdf). The current measurement studies about emission characteristics and chemical

123   composition of CPM exhibited non-negligible emissions. For example, Yang et al. (2014, 2018a, 2018b)

124   conducted investigations for different types of industrial boilers and power plants, and concluded that

125   CPM constituted 25.7~96.5% of $PM_{2.5}$. For an ultralow-emission coal-fired power plant, Li et al. (2017b)

126   reported that the emission concentrations of CPM accounted for 83% of the $PM_{2.5}$. Wang et al. (2018)

127   calculated the average emission factors of CPM from two stacks in a waste incineration power plant to

128   be 0.201 and 0.178 g/kg, which were 22.0 and 31.2 times higher than the corresponding those of FPM,

129 respectively. Wu et al. (2020) found that FPM emissions from four typical coal-fired power plants met

130 Chinese ultra-low emission standards, while CPM showed high levels (even above 10 mg/Nm^3). CPM

131 includes organic and inorganic components, known as organic CPM and inorganic CPM, respectively.

132 The contributions of organic fractions varied from 13.6% to 80.5%, depending on different fuel types,

133 test methods and operating conditions (Lu et al., 2019; Song et al., 2020; Yang et al., 2021, 2018b). Many

134 studies confirmed that more than 50% of organic composition were measured in CPM (Li et al., 2017c,

135 2017d; Song et al., 2020; Wu et al., 2020), revealing that organic matter comprising a large proportion in

136 CPM needed to be taken into account. These above studies provided valuable basic information of CPM

137 emission characteristics for data references in this study, as summarized in Table S3. It is likely that the

138 inorganic fractions of CPM make a contribution to the water-soluble ions in PM$_{2.5}$, and organic

139 components contribute to the organic matter in PM$_{2.5}$. In addition, large amounts of low volatile organic

140 compounds in CPM can be important precursors for SOA formation.

141 Current measurement methods for PM in stationary exhaust sources in China (GB/T 16157-1996)

142 have not involved the collections of CPM; and the chemical composition of collected PM was quite

143 different from that actually released into the atmosphere (Hu et al., 2016). The emission inventory

144 constructed based on emission surveys did not include the CPM emissions. So it is important to introduce

145 CPM emissions to the current emission inventory. For example, a European study improved OA

146 simulations by including the CPM emissions from residential wood combustion sources (Van Der Gon et

147 al., 2015). Morino et al. (2018) revised the emission inventory by the consideration of CPM in Japan and

148 showed that the OA emission rates were up to seven times the previous ones and CPM contributed largely

149 to atmospheric OA concentrations. A shortcoming of that study was that it did not separate the effects of

150 CPM emissions on POA and SOA concentrations. Moreover, studies still lack quantification of emissions

151 of CPM released by stationary combustion sources in China.

152 In this study, we use the available CPM emission information to construct an emission inventory of

153 CPM from stationary combustion and mobile sources in China (with a focus on OA) and conducted 15

154 sensitivity simulations to explore the contributions of CPM emissions to atmospheric OA and PM$_{2.5}$

155 concentrations during the winter haze episodes over China. This quantitative study about organic CPM

156 emissions and the roles of CPM in the OA formation emphasizes the importance of constraining CPM

157 emissions from stationary combustion and mobile sources.

158

159 **2 Materials and methods**

2.1 Estimations of CPM emissions

160

161 We collected available emission measurement data of CPM based on published literatures. Totally,

162 CPM emission data from 52 stationary combustion sources were acquired (Table S3). The emission

163 sectors for these data included coal-fired power plants, waste incineration power plants, industrial coal

164 boilers, heavy oil boilers, wood boilers, natural gas boilers, diesel boilers, iron and steel plants, and

165 incinerators. Emissions of CPM depend on many factors including source categories, fuel types, sampling

166 flue gas temperature, and air pollution control devices (Feng et al., 2021). Also, different measurement

167 methods produced different results of CPM emissions (Wang et al., 2020a). Recently, cooling and dilution

168 methods have been applied to monitor CPM concentrations. The emission rate of OA in CPM was

169 estimated as follows in Eq. (1) and (2) (Morino et al., 2018):

170
$$E_{OA}(CPM) = \sum A \times EF_{OA}(CPM) = \sum A \times EF_{PM2.5}(FPM) \times \frac{EF_{OA}(CPM)}{EF_{PM2.5}(FPM)} \quad (1)$$

171
$$E_{OA}(CPM) = \sum E_{PM2.5}(FPM) \times \frac{C_{OA}(CPM)}{C_{PM2.5}(FPM)} \quad (2)$$

172
$$E_{OM_{lsi}}(CPM) = E_{OA}(CPM) \times \frac{E_{OM_{lsi}}(CPM)}{E_{OA}(CPM)} = E_{OA}(CPM) \times \frac{C_{OM_{lsi}}(CPM)}{C_{OA}(CPM)} \quad (3)$$

173 Where E_{OA}(CPM) is the emission rate of organic matter in CPM; EF_{OA}(CPM) is the emission factor of

174 organic matter in CPM; $E_{PM2.5}$(FPM) is the emission rate of FPM$_{2.5}$; $EF_{PM2.5}$(FPM) is the emission factor

175 of FPM$_{2.5}$; A denotes the activity level; C_{OA}(CPM) is the concentration of organic matter in CPM; and

176 $C_{PM2.5}$(FPM) is the concentration of FPM$_{2.5}$. Among these parameters, C_{OA}(CPM) and $C_{PM2.5}$(FPM) were

177 derived from the collected emission survey data at the above stationary sources. The ratios of C_{OA}(CPM)

178 to C_{OA}(FPM) can be used to estimate E_{OA}(CPM), but due to the limited data and very low values of

179 C_{OA}(FPM) at stationary sources, $C_{PM2.5}$(FPM) was used instead of C_{OA}(FPM). The ratios of E_{OA}(CPM) to

180 $E_{PM2.5}$(FPM) and EF_{OA}(CPM) to $EF_{PM2.5}$(FPM) should be equal to the ratios of C_{OA}(CPM) to $C_{PM2.5}$(FPM)

181 at the same dilution ratio in the emission surveys, as summarized in Table 1. In this estimate, these

182 emission ratios collected from the best available data from the stationary sources were applied to represent

183 the stationary combustion sources in the current emission inventory. A and $EF_{PM2.5}$(FPM) in Eq. (1) were

184 combined to get $E_{PM2.5}$(FPM) in Eq. (2), acquired from PM$_{2.5}$ emission rates in the emission inventory of

185 baseline year. The organic CPM mainly contains alkanes (with C$_{10}$-C$_{30}$ being the major n-alkanes), esters,

186 and polycyclic aromatic hydrocarbons (PAHs) (Li et al., 2017c, d; Song et al., 2020; Zheng et al., 2018).

187 Based on the relationship between carbon number of n-alkanes and saturation concentrations (C*)

188 following Lu et al. (2018), it is reasonable to speculate that organic CPM is composed of organic matter

Atmospheric
Chemistry
and Physics
Discussions

Open Access

EGU

189   which has low volatility (LVOC, $10^{-3}<C^*<10^0$), semi-volatile (SVOC, $10^0<C^*<10^3$), or has intermediate

190   volatility (IVOC, $10^3<C^*<10^6$), combined as OM_{lsi} (CPM). Since the volatility characteristics of organic

191   CPM from stationary sources have not been accurately determined in relevant measurement studies, the

192   emissions of OM_{lsi} (CPM) were scaled to emissions of OA (CPM) in this estimate as shown in Eq. (3).

193   E_{OMlsi} (CPM) is the emission rate of OM_{lsi} in CPM; C_{OMlsi} (CPM) is the concentration of OM_{lsi} in CPM.

194   The specific partition coefficients for different volatility bins in the model will be discussed in the

195   following Sect. 2.3. In addition to stationary sources, mobile sources also generate certain emissions of

196   CPM. Due to the lack of CPM emission data from on-road and off-road vehicles, we increased OA

197   emission rates of the transportation sector (TR) by 30% to consider the contributions of CPM from these

198   sources, following Morino et al. (2018) and Lu et al. (2020).

199

200   **2.2 The model configuration**

201   The three-dimensional Community Multiscale Air Quality (CMAQ, v5.3.2) model developed by the

202   U.S. Environmental Protection Agency was used to simulate spatiotemporal distributions of chemical

203   species. The detailed model configuration can be referred to Appel et al. (2021) and Yu et al. (2014). The

204   gas-phase chemical mechanism was based on the Carbon Bond Mechanism 6 (CB6) scheme. The aerosol

205   module was based on the seventh-generation aerosol module of CMAQ (AERO7). The CMAQv5.0.2-

206   VBS version with AERO6 coupled with a VBS module (AERO6VBS) was used for comparison.

207   Compared to the SOA formation in AERO6 in the CMAQv5.2, the AERO7 module includes

208   improvements: enhanced consistency of the SOA formation pathways between chemical mechanisms

209   based on CB and SAPRC, updated photooxidized monoterpene SOA yields (Xu et al., 2018), added

210   uptake of water by hydrophilic organics (Pye et al., 2017), consumption of inorganic sulfate when forming

211   isoprene epoxydiol organic sulfate (Pye et al., 2013), and replacement of the Odum two-product model

212   with a VBS framework to parameterize SOA formation (Qin et al., 2021; Appel et al., 2021). Both

213   AERO6VBS and AERO7 contained five classes of organic matter with one class being nonvolatile and

214   the other four classes being semi-volatile with effective saturation concentrations of 1, 10, 100, and 1000

215     $\mu g\ m^{-3}$. Each of these volatility bins was assigned to the CMAQ species of LVPO1, SVPO1, SVPO2,

216   SVPO3 and IVPO1, respectively. The emissions of unspeciated IVOC were set equal to 1.5 times the

217   POA emissions in AERO6VBS and 6.579 times in AERO7 by default (Table 3). The high scale factor of

218   6.579 in AERO7 was set to consider missing pathways for the SOA formation from combustion sources

219   including the IVOC oxidation (Murphy et al., 2017; Murphy et al., 2021), and it was primarily

Atmospheric
Chemistry
and Physics
Discussions
Open Access
EGU

220   parameterized in Los Angeles where vehicle emissions are a principal source (Hayes et al., 2015). This

221   parameter setting may not be suitable for fire and wood-burning sources and might have accounted for

222   the CPM contributions. In addition, the ratios of C_{SIVOCs} to C_{OA} can be dependent on C_{OA} under stack

223   conditions, which were generally above 3000 μg m^{-3} in CPM according to the emission surveys.

224   Considering high OA concentrations, we revised the scale factor of IVOC to 1.5 (same as that in

225   AERO6VBS) in the AERO7_adj case which was regarded as the base case. Meteorological fields were

226   predicted by the Weather Research and Forecasting (WRF) model version 3.7. The physical schemes of

227   WRF were the same as those in Wu et al. (2018) and Zhang et al. (2021). Meteorological initial and

228   boundary conditions were provided by the National Center for Environmental Prediction (NCEP) final

229   analysis dataset with the spatial resolution of 1°×1° and temporal resolution of 6 h. The first several days

230   were used for model spin-up, varied for different pollution periods as described in Sect. 2.4. The gridded

231   anthropogenic emission data for 2014 and 2017 were derived from Emission Inventory of Air Benefit and

232   Cost and Attainment Assessment System (EI-ABaCAS) developed by Tsinghua University (Dong et al.,

233   2020; Zheng et al., 2019). It contained primary species such as PM$_{2.5}$, SO$_2$, NO$_x$, CO, NMVOCs, NH$_3$,

234   BC, and OC from nine anthropogenic sectors (i.e., agriculture, power plant, industry process, industry

235   combustion, steel, cement, residential, transport, and open burning). Biogenic source emissions were

236   calculated by on-line Biogenic Emission Inventory System version 3.14 (BEISv3.14) model (Carlton and

237   Baker, 2011). Dust emissions were calculated by an on-line windblown dust scheme (Choi and Fernando,

238   2008). Our study period in 2014 occurred before and during the Asia-Pacific Economic Cooperation

239   (APEC) summit held in Beijing (November 5–11, 2014). During the period of pre-APEC (October 28–

240   November 2) and full-APEC (November 3–11), some pollution control measures were gradually

241   implemented in Beijing and its surrounding areas. Thus we conducted emission reduction by 30% during

242   the above time period for two municipalities (Beijing and Tianjin), four provinces (Hebei, Shanxi, Henan,

243   and Shandong), and Inner Mongolia Autonomous Region (Li et al., 2017e, 2019). The simulation domain

244   covered mainland China by a 395 × 345 grid with the horizontal grid resolution of 12 km (Fig. 1). There

245   were 29 vertical layers in σ$_z$ coordinate system reaching the upper pressure (100 hPa) with 20 layers

246   located in the lowest 3 km to resolve the planetary boundary layer.

247

248   **2.3 Design of sensitivity simulation cases**

249   According to the emission parameters summarized in Table 1, we carried out bootstrapping and

250   Monte Carlo simulations to obtain the mean and uncertainty ranges of E$_{OA}$(CPM)/E$_{PM2.5}$(FPM) for

251 stationary combustion sources including power plant (PP), industry combustion (IN), steel (IR) (see Table

252 2). First, the optimal probabilistic distributions and uncertainty ranges were determined for each source

253 category. Then the statistical bootstrap simulation was applied to calculate the mean and 95% confidence

254 interval of emission ratios for each source category. Finally, the uncertainties of these parameters were

255 propagated to calculate the total uncertainty of emission by running Monte Carlo simulations for 10,000

256 times. On this basis, a series of sensitivity cases including low, medium, and high emission ratios were

257 designed to explore the contributions of CPM emissions to OA concentrations and quantify uncertainty

258 ranges of CPM effects on OA (Table 3).

259   Here, to explore the contributions of organic CPM emissions to atmospheric OA and $PM_{2.5}$

260 concentrations, the estimated emissions of organic CPM were added into the CMAQ model as an

261 individual source, separated from other emission sources. For the base scenarios, the simulations were

262 performed with the input of the previous emission inventory without the newly constructed organic CPM

263 emissions in the AERO6VBS, AERO7_def and AERO7_adj cases. Except the revision of scale factor of

264 IVOC in AERO7_adj case, the rests were kept at the default settings in the model. On the other hand,

265 different volatility distributions could be chosen for different emission sources, but this was not our study

266 focus and did not interfere with the results of CPM contributions. For the other cases including CPM

267 emissions from stationary combustion sources, the emissions of organic CPM were mapped to surrogate

268 species of different volatility bins (LVPO1, SVPO1, SVPO2, SVPO3, and IVPO1) in the CMAQ model.

269 Due to the unavailable volatility distribution information of OM_{lsi} (CPM), different scaling factors of

270 volatility bins were employed under each emission scenario to discuss the uncertainty of CPM effects. In

271 this study, we tested two kinds of scaling factors for the five volatility bins of SVOC: fac1 (0.09, 0.09,

272 0.14, 0.18, 0.5) (Grieshop et al., 2009), fac2 (0.40, 0.26, 0.40, 0.51, 1.43) (Shrivastava et al., 2011). The

273 fac2 estimated total SVOC emissions as 3 times POA emissions to consider missing OM_{lsi} (CPM)

274 emissions. Although the high coefficient settings may lead to overestimation of the simulations, it was

275 still applied to discuss the sensitivity of modeling results to different volatility distributions. Then the fac3

276 (0.245, 0.175, 0.27, 0.345, 0.965) which is the average of fac1 and fac2, was also tested for the SVOC

277 volatility bins under which the IVOC scale factor was set to 2.5. The fac1, fac2, and fac3 were applied to

278 the OM_{lsi} (CPM) emissions for cases S1.1, S1.2, and S1.3, respectively (see Table 3). For an evaluation

279 of the sensitivity of OA outputs to organic CPM emissions, we conducted simulations with different

280 magnitudes of CPM emissions at the 95% and 50% confidence interval. Thus the S2-S3 cases were

281 designed with the uncertainty ranges of $E_{OA}(CPM)/E_{PM2.5}(FPM)$ at 95% confidence interval (73% and

282 128% of the amounts in S1), and the S4-S5 cases with the uncertainty ranges at 50% confidence interval

283 (90% and 109% of the amounts in S1). Moreover, the contributions of individual emission categories

284 including PP, IN, IR, and TR were quantified by excluding perturbation of other sources in the S6-9 cases.

285 The simulated contributions of CPM emissions to POA, SOA, OA, and $PM_{2.5}$ concentrations were

286 calculated as the improved concentrations after including CPM emissions relative to the base case under

287 these scenarios.

2.4 Observational data

290   For the year 2014, the simulation period was from October 6 to November 14, 2014, with the first 8

291 days being the model spin-up time. Field observation data during the episode from October 14 to

292 November 14, 2014, at the Institute of Atmospheric Physics (IAP) (39°58′ N, 116°22′ E) in Beijing were

293 from Li et al. (2017a) and Xu et al. (2015). Concentrations of aerosol components were measured in PM_1.

294 In order to make a comparison between simulated and observed results, the $PM_1/PM_{2.5}$ ratio of 0.77 was

295 used to calculate the observed component concentrations in $PM_{2.5}$ based on the observations from Xu et

296 al. (2015). Observation data of organic carbon (OC) on November 3, 2014, at Qianyanzhou (located in

297 Jian city) and Changsha were provided by CERN Atmospheric Science Branch of the Institute of

298 Atmospheric Physics, Chinese Academy of Sciences (Liu et al., 2018). For the year 2018, the simulation

299 period included December 1 to 31, 2018, with the first 5 days for model spin-up. The observation values

300 of OC in the BTH2+26 cities were provided by China Environmental Monitoring Station. These cities

301 include Beijing, Tianjin, Anyang, Baoding, Binzhou, Cangzhou, Changzhi, Dezhou, Hebi, Handan,

302 Hengshui, Heze, Jincheng, Jinan, Jining, Jiaozuo, Kaifeng, Liaocheng, Langfang, Puyang, Shijiazhuang,

303 Tangshan, Taiyuan, Xingtai, Xinxiang, Yangquan, Zibo, and Zhengzhou. The OA/OC ratio of 1.4 (Simon

304 et al., 2011) was used to calculate OA concentrations for the comparison with the simulation results. The

305 observed concentrations of $PM_{2.5}$ were collected from the Chinese National Environmental Monitoring

306 Center (CNEMC). Since the $PM_{2.5}$ observation data from December 22 to 26 were missing, the following

307 analysis of $PM_{2.5}$ did not include these five days. The hourly observation data of meteorological factors,

308 including temperature (T), relative humidity (RH), wind speed (WS), and wind direction (WD), were

309 provided by the China Meteorological Administration (http://data.cma.cn/site/index.html).

3 Results and discussion

3.1 Emissions of condensable particulate matter

313   Emissions of OA in CPM (E_{OA}(CPM)) were comparable to or even exceeded the emissions of

314   filterable $PM_{2.5}$ ($E_{PM2.5}$(FPM)) for most stationary combustion sources, regardless of the differences

315   among these values (Table 1). Therefore, we constructed a new emission inventory by including CPM.

316   The annual emissions of OA in previous and modified emission inventory over China for the year 2014

317   and 2017 are presented in Fig. 2. The OA represents the organic matter in the emission input before the

318   further volatility distributions, while OM ($C^* \leq 100$) represents the organic matter allocated in the bin of

319   C^* equal to 10 and below after application of the volatility distributions for the fac1, fac2 and fac3 cases.

320   Based on the simulation case settings, OA (FPM) from all the sectors was multiplied by fac1 (0.5), while

321   OA (CPM) from stationary combustion and mobile sources was multiplied by fac1 (0.5), fac2 (1.57) or

322   fac3 (1.035). In the previous inventory for 2014 without CPM, the emissions of OA were 3664.6 Gg,

323   approximately equal to 40% of $PM_{2.5}$ emissions. After the inclusion of CPM released by stationary

324   combustion sources in the new inventory, the emissions of OA were enhanced by a factor of 2 and even

325   exceeded emissions of $FPM_{2.5}$. The dominant contributors of OA (FCPM) are combustion sources in

326   power plant and industrial sectors, estimated to be 66% (7006.2 Gg) of the total OA emissions

327   (10531.1Gg). The emissions of OM ($C^* \leq 100$) remained unchangeable for the open burning, domestic,

328   and industry process sources since they were mostly FPM, while OM ($C^* \leq 100$) for the power plant,

329   industry combustion, and steel sources were variable based on whether fac1, fac2 or fac3 were applied

330   to the CPM. Similarly, the emissions of OA (FCPM) were 3 times those of OA (FPM) for the year 2017.

331   The emissions of OA from power plant, industry combustion, and steel sources increased by 33 times

332   after considering CPM emissions. These results indicate that the inclusion of organic CPM from

333   stationary combustion sources has a major impact on OA emissions and improves contributions of

334   industrial and power sectors to OA emissions.

335   Notably, the emission estimates of OA in CPM contained uncertainties, mainly attributed to the

336   representativeness and limitations of chosen emission sources. For power plant, industry combustion, and

337   steel sectors, the average ratios of E_{OA}(CPM) to $E_{PM2.5}$(FPM) were 4.12, 1.38 and 2.80, respectively (Table

338   2). Overall, the uncertainty range of E_{OA}(CPM) related to variabilities in the ratio of E_{OA}(CPM) to

339    $E_{PM2.5}$(FPM) was -27% ~ +28% at the 95% confidence interval. On this basis, a series of sensitivity cases

340   with different emission ratios were set to determine the uncertainty ranges of CPM contributions (Table

341   3). In the future, actual measurements of organic CPM emissions from various sources and source-specific

342   identification of volatility distributions are needed to reduce uncertainties in emission estimates.

343

3.2 Meteorological evaluation

Comparisons between simulated and observed hourly meteorological variables including T, RH, WS, and WD from October 14 to November 14, 2014, at the Beijing site are displayed in Fig. S1. Results show that the model reproduced the hourly variations of T and RH reasonably well, although the maximum and minimum T, and RH did not totally match the observed values. The simulated WS were overestimated, but the hourly changes were reproduced. The variations of WD were not well captured, but the magnitudes of simulated WD were consistent with the observations over the whole period. A more detailed model evaluation for meteorological variables during October 14 –November 14, 2014 and December 1–30, 2018 at 9 cities over China is given in Table S1. MB, GE, RMSE denote the bias, root mean square error, and fractional error, respectively, and R refers to the correlation coefficient between observed and simulated results. For the Beijing site in 2014, the MB of T was -0.3 □, indicating a small deviation of modeled temperature. Good correlations between simulation and observation were shown for T, RH, and WS with R values of 0.90, 0.75, and 0.62, respectively. For all these cities, T, RH, and WS had the R values of 0.83~0.94, 0.67~0.89, and 0.21~0.70 during the study period in 2014, respectively. The R values for T, RH, and WS in 2018 were 0.74~0.95, 0.52~0.85, and 0.33~0.75, respectively. The GE and RMSE of WS were lower than model performance criteria (2 m/s) (Emery et al., 2001) for most cities, displaying relatively good simulations of wind speed. In summary, the WRF model showed a relatively consistent simulation performances of meteorological variables.

3.3 Effects of CPM emissions on POA and SOA concentrations

For the hourly observed and simulated SOA and POA concentrations at the Beijing site, Figs. 3 and 4 show obvious improvements of SOA and POA levels after the consideration of CPM contributions. The specific model species for POA and SOA are shown in Table S4. In all the simulation scenarios, five complete ascending and descending SOA episodes in Fig. 3 were well captured, with much lower mean bias between observations and simulations than previous results of Li et al. (2017a). Three pollution episode processes before the APEC were clearly captured by the model. The third process (October 27– November 1) had lower observed SOA levels relative to the first (October 16–21) and second processes (October 22–26), attributed to lower precursor emission concentrations, lower temperature, and regional transports by strong northerly winds on October 26. During the APEC, there were two pollution episodes with lower SOA concentrations due to the effects of emission controls and meteorological conditions (Ansari et al., 2019; Liang et al., 2017). Compared to the observed values, cases without CPM exhibited

375 varying degrees of overestimation or underestimation for SOA and POA. For example, in the AERO7_def

376 case, the maximum SOA values were overestimated by 42% in the first episodes and up to 67% in the

377 third episodes, while the POA values were largely underestimated by an average of 73% during the whole

378 time period. Then we revised the scale factor of IVOC in the AERO7_adj case (see Table 3). The

379 overestimated SOA in the AERO7_def for the first and third episodes were reduced by 65% and 60%,

380 respectively. In comparison, the AERO6VBS case underpredicted SOA by up to 65%, and simulated low

381 levels of POA during the first three periods and high levels in the last two episodes. The base case in the

382 following discussions referred to AERO7_adj. Overall, the base case underestimated the average POA

383 and SOA levels by 76% and 66% (Table 4), respectively, emphasizing the potential contributions of

384 missing CPM sources.

385   After considering CPM emissions, the underestimation of average POA and SOA was reduced to 38%

386 and 24% under the S1.1 scenario, respectively (Table 4). From the simulated hourly variations in the S1.1

387 case (Fig. 3), SOA concentrations were enhanced by factors of 0.01~3.10 relative to base case, more

388 consistent with the observations. The gap between average simulations and observations decreased from

389 -11.56 to -4.23 $\mu g\ m^{-3}$ (63% decrease). For the peak values in the first, second, fourth, and fifth pollution

390 episodes, the improvements in the peak SOA concentrations were approximately 30, 30, 10, and 15 μg

391 m^{-3}. Nevertheless, the overestimation of SOA occurred in the third process, mainly due to meteorological

392 conditions considering the fact that the observed and modeled wind directions were inconsistent during

393 this period as shown in Fig. S1. The prevailing southerly and northeast wind directions in the model

394 during the third process did not bring clean air from the northwest boundary to dilute the local generated

395 SOA (Li et al., 2016, 2019). Also, higher simulated wind speeds transported more precursors with the

396 southerly and northeast winds and caused the overestimation of SOA (see Fig. S1). Correspondingly, the

397 hourly POA simulation concentrations in the S1.1 case increased by 0.13~4.55 times compared to the

398 base case, narrowing the average gap between simulations and observations from -12.29 to -6.14 $\mu g\ m^{-3}$

399 (50% decrease), but the high observed levels of POA were still not attained under this scenario.

400 Comparatively, the S1.2 case presented similar hourly simulation results of SOA to the S1.1 case with the

401 enhancement by factors of 0.02~3.77 versus the base case, while the simulated POA values were nearly

402 1.3 times higher than the S1.1 case, capturing most of the high observations throughout the whole study

403 period. This demonstrates that the SVOC parameters had more impact on POA than SOA. Under the S1.3

404 scenario using different SVOC and IVOC parameters from the S1.2 case, the simulation concentrations

405 of SOA were 24% higher and POA were 29% lower than those under the S1.2 scenario as shown in Table

406   4. Based on the evaluation results, the S1.3 scenario showed the optimal improvement effects, with the

407   mean biases of 1.16% for POA and 2.16% for SOA (see Table 4). In consideration of the uncertainty

408   ranges of CPM emissions, a series of sensitivity cases with different emission ratios were conducted.

409   Under the minimum emission scenario in the S2.1 case, the average SOA and POA concentrations were

410   14.4%, and 16.5% lower than those in the S1.1 case, respectively. Under the maximum emission scenario

411   in the S3.1 case, the average SOA and POA concentrations were 14.6% and 17.3% higher than those in

412   the S1.1 case, respectively. Thus the model can resolve 62% (52%~73%) of the observed POA

413   concentrations and 76% (65%~87%) of the observed SOA concentrations in the cases S1.1 (S2.1, S3.1).

414   Then the S2.2 and S3.2 cases applied the same S/IVOC parameters as S1.2, and also displayed similar

415   results of SOA to those in the S2.1 and S3.1 cases, respectively. Under this setting, the uncertainty ranges

416   were -14.6% to +14.5% for SOA, and -22.8% to +23.9% for POA in the S1.2 case as shown in Table 4.

417   For the S4.2 and S5.2 cases with the CPM emissions at 50% confidence interval, their SOA concentrations

418   showed small changes with 5.3% lower in the S4.2 case and 4.7% higher in the S5.2 case than the S1.2

419   case; similar minor sensitivity of 8.5% decrease (S4.2) and 7.6% increase (S5.2) were found for POA. To

420   explore the contribution of each source category to SOA and POA and identify the key anthropogenic

421   sources of CPM, we conducted simulations with the different separate inputs (S6~S9) (see Table 3).

422   Results show that the CPM emissions from the IR sector made the largest contribution to the POA and

423   SOA increases, accounting for 59% of POA and 55% of SOA, followed by PP (26% for POA and 30%

424   for SOA) and IN sources (13% for POA and 14% for SOA). This was consistent with the differences in

425   the CPM emissions from the above three source sectors (Fig. 2). The sensitivities of SOA and POA to the

426   emission ratio of organic CPM from the TR sector were very small, indicating a weak impact on OA due

427   to small contributions of transportation sources to the OA emissions in FCPM. The above results

428   demonstrate that CPM from stationary sources was an important source for both POA and SOA formations.

429   In summary, when considering the uncertainties of organic CPM emissions, CPM can be a significant

430   contributor to OA concentrations, with the contributions of 61% (53%, 67%) to POA, 55% (48%, 61%)

431   to SOA, 58% (50%, 63%) to OA under the S1.1 (S2.1, S3.1) scenario, and 83% (78%, 86%) to POA, 59%

432   (52%, 64%) to SOA, 74% (67%, 78%) to OA under the S1.2 (S2.2, S3.2) scenario. The S1.3 scenario had

433   the best improvement performance with CPM contributing 76% to POA, 67% to SOA, and 71% to OA.

434   Because of the better representations of temporal variations of SOA and POA after including CPM

435   emissions, OA simulations were correspondingly improved. To separate the effects of CPM on OA into

436   different process contributions, we compared simulation results of these sensitivity cases as shown in Fig.

437　　5. The OA composition contains POA, ASOA (SOA from anthropogenic VOCs), BSOA (SOA from

438　　biogenic VOCs), and SISOA (SOA from low volatile S/IVOCs). The difference between simulations and

439　　observations decreased from 23.84 $\mu g\, m^{-3}$ in the base case to 10.37 $\mu g\, m^{-3}$ in the S1.1 case (56% decrease),

440　　with the uncertainty of 13.95 $\mu g\, m^{-3}$ (41% decrease in S2.1) to 6.69 $\mu g\, m^{-3}$ (72% decrease in S3.1) relative

441　　to the base case. However, these cases still underestimated the observed OA levels. The S1.2, S2.2 and

442　　S3.2 cases increased the contributions of CPM to OA by 14.01, 10.24, 17.92 $\mu g\, m^{-3}$, with the percentage

443　　increases of 60%, 52%, 66% compared to S1.1, S2.1 and S3.1, respectively. Notably, the average OA

444　　simulations were the closest to the observations in S1.3, with the average CPM contributions of 24.41 μg

445　　m^{-3} and a minor overestimation of 1.68% (see Table 4). Taking OA composition into account, POA and

446　　SISOA accounted for the largest part in all these scenarios. The effects of CPM were only reflected in the

447　　enhancements of POA and SISOA. These results suggest that OA was sensitive to the emissions of CPM

448　　and S/IVOCs, so it is required to reduce emission uncertainties for better simulations. To sum up, the

449　　revised simulations after the inclusion of CPM from stationary combustion and mobile sources led to

450　　improved modeling performances of OA during the winter haze episodes, revealing a significant

451　　contribution of CPM to atmospheric OA.

452

453　**3.4 Effects of CPM on OA and PM$_{2.5}$ concentrations**

454　　To ensure the accuracy and reliability of our modeling results, further studies in other cities were

455　　presented. Fig. 6 shows large contributions of CPM to OA on November 3, 2014, at Changsha and

456　　Qianyanzhou. After the inclusion of CPM effects in the S1.1, S1.2 and S1.3 cases versus the base case,

457　　the simulated OA concentrations were improved by 96.4%, 198.3% and 142.1% for Changsha,

458　　respectively. The simulated OA concentrations increased by 129.7%, 243.1% and 199.1% in the S1.1,

459　　S1.2 and S1.3 cases versus the base case for Qianyanzhou, respectively. Comparatively, the S1.2 case

460　　contributed to greater increases of OA concentrations, narrowing the simulation-observation bias from

461　　80% to less than 40% for Changsha and more than 70% to less than 25% for Qianyanzhou. The remaining

462　　bias was probably attributed to the effects of meteorological factors.

463　　The impacts of CPM on OA were studied during December 6–30, 2018, in the BTH 2+26 cities.

464　　Likewise, the improvements in daily OA simulation concentrations can be found at the four studied cities

465　　after the consideration of CPM, especially for high pollution days (Fig. 7). The modeled underestimations

466　　of OA were improved from -68% to -28%, -63% to -13%, -75% to -36%, and -71% to -33% with the

467　　inclusion of CPM emissions in the S1.1 case relative to the base case for Handan, Shijiazhuang, Xingtai

468   and Dezhou, respectively (Table 4). The contributions of CPM emissions to total OA concentrations

469   reached up to 55%, 58%, 60%, and 57% for Handan, Shijiazhuang, Xingtai, and Dezhou, respectively.

470   Under the S1.3 scenario, the OA simulations showed greater increases, and slightly exceeded observation

471   values with the mean biases of 10%, 40%, 2%, and 3% for the above four cities, respectively. For example,

472   daily OA levels in Handan increased by 5.7~59.3 $\mu g\ m^{-3}$ after including CPM effects (S1.1 versus base

473   case). On average, CPM contributed to the increases in OA concentrations by 1.2 times. However, some

474   observations were not captured, while the observed value on December 20 was overestimated, indicating

475   uncertainties of the estimated organic CPM emissions. Under the S1.3 scenario, the average simulated

476   OA concentrations were enhanced by 2.4 times relative to the base case, with a good capture of some

477   underestimated values in the S1.1 case. For Shijiazhuang with daily OA concentrations below 80 $\mu g\ m^{-3}$,

478   the base case underestimated OA levels by 10~84%. After incorporating the CPM emissions in the S1.1

479   case, the daily OA concentrations were significantly improved by factors of 0.8~2.0. Some observed high

480   values of OA were well captured in the S1.1 case on December 10 with the simulation of 64.6 $\mu g\ m^{-3}$

481   versus observation of 58.6 $\mu g\ m^{-3}$, and on December 14 and 30. Under the S1.3 scenario, the daily OA

482   levels increased by factors of 1.7~4.4 relative to the base case. Although the average OA concentrations

483   were somewhat overestimated in the S1.3 case, good agreements between observations and simulations

484   existed on some days, including December 9, 12, 13, 16-19, and 24. For Xingtai, the simulated OA

485   concentrations were enhanced by factors of 1.2~2.4 in the S1.1 case relative to the base case. The model

486   can resolve 64% of average OA observations in the S1.1 case when the emissions of CPM were included.

487   The average OA simulation value was improved by 32.5 $\mu g\ m^{-3}$ in the S1.3 case compared to the base

488   case. Then Dezhou showed similar results with the enhancement of 1.0~2.2 times for daily OA contributed

489   by CPM in S1.1. Although the observed high OA concentrations exceeding 80 $\mu g\ m^{-3}$ on December 11

490   and 16 were not captured in the S1.1 case, the bias between simulations and observations was reduced to

491   -27.2 and -31.2 $\mu g\ m^{-3}$ versus -65.1 and -58.6 $\mu g\ m^{-3}$ in the base case, respectively. The underestimations

492   of high OA levels on December 11 and 16 were resolved in the S1.3 case, and the average concentrations

493   over the whole period were very close to the observations. Table S2 shows the model evaluation results

494   for $PM_{2.5}$ concentrations under different sensitivity simulation cases. Dezhou was not included due to the

495   missing data. After including the CPM emissions in the S1.1 case, the model can resolve 83%, 83%, and

496   69% of average $PM_{2.5}$ observations with increases in $PM_{2.5}$ concentrations by 35%, 40%, and 41% relative

497   to the base case for Handan, Shijiazhuang, and Xingtai, respectively. $PM_{2.5}$ simulations were further

498   enhanced for these four cities in the S1.3 case with the NMB values of 3%, 8%, and -11%, respectively.

499   It was notable that the emissions of inorganic components in CPM were not investigated in this study,

500   which can cause modeling deviation. Other factors including boundary layer height and wind can also

501   affect the simulations. In summary, our estimated CPM emissions showed a reasonable range, which can

502   make a significant contribution to atmospheric OA and $PM_{2.5}$.

503

3.5 Regional contributions of CPM to OA and $PM_{2.5}$

505   The regional effects of CPM emissions on atmospheric OA and $PM_{2.5}$ from a nationwide perspective

506   were investigated. The concentrations of POA, SOA and OA averaged over the whole study period from

507   October 14 to November 14, 2014, showed varying degrees of regional increases after incorporating CPM

508   emissions, mainly in central and eastern regions in China (Fig. 8). In the base case, the simulation values

509   of POA and SOA were both lower than 14 µg m^{-3} over China. Correspondingly, OA concentrations did

510   not exceed 22 µg m^{-3} with the maximum values distributed in the BTH region and Central China. After

511   the consideration of CPM effects in the S1.1 case relative to the base case, the concentrations of POA,

512   SOA and OA substantially increased over North China, East China, and Central China including Beijing,

513   Tianjin, Shanghai, and provinces of Liaoning, Shandong, Shanxi, Henan, Hubei, Anhui, Jiangsu, Zhejiang,

514   Hunan, Jiangxi. The most remarkable enhancement values were up to 10, 12, and 20 µg m^{-3} for POA,

515   SOA and OA, respectively. Then under the S1.2 scenario with the same emissions as the S1.1 case but

516   different SVOCs parameterization, substantial increases in the POA simulations by more than 16 µg m^{-3}

517   were found for most cities in North China, East China, and Central China, with the maximum distributed

518   in the BTH region (up to 24 µg m^{-3}), attributable to large amounts of emissions from industrial plants and

519   power plants in this region. The OA concentrations for many cities located in North China and East China

520   increased by more than 24 µg m^{-3} after including CPM emissions in the S1.2 case. Since the contributions

521   of CPM to SOA in the S1.2 case were only slightly larger than those in the S1.1 case, the greater

522   improvements of OA in S1.2 mainly result from the POA increases. The S1.3 case used different S/IVOCs

523   parameterizations from the S1.2 case, with the regional contributions of CPM emissions to POA and SOA

524   lower and higher than those in S1.2, respectively. The regional increases in the POA, SOA and OA

525   simulations in the S1.3 case were not lower than 10, 12, and 20 µg m^{-3} for most cities in North China,

526   East China, and Central China, respectively.

527   The regional contributions of CPM emissions to $PM_{2.5}$ concentrations were explored in the

528   BTH2+26 cities averaged over the period from December 6 to 30, 2018 (Fig. 9). In the base case without

529   the CPM effects, the model comparisons against observations suggest that $PM_{2.5}$ levels were greatly

530   underestimated in almost all cities except Tangshan (Fig. 9a). Several cities with observed PM$_{2.5}$

531   concentrations higher than 80 µg m^{-3} showed the greatest underestimations with simulation values under

532   50 µg m^{-3}. Under the S1.1 scenario including CPM emissions, the simulated PM$_{2.5}$ concentrations were

533   substantially enhanced in almost all the studied cities, closer to the observations (Fig. 9b). The

534   contributions of CPM to PM$_{2.5}$ were not lower than 14 µg m^{-3} for the most cities (Fig. 9c). Under the S1.3

535   scenario, CPM made a significant contribution to PM$_{2.5}$ concentrations, more than 26 µg m^{-3} for most

536   cities (Fig. 9f). High observations for Baoding, Shijiazhuang, Xingtai, Hengshui, Dezhou and Handan

537   were well captured (Fig. 9e). The scatter plots of observed and simulated daily PM$_{2.5}$ concentrations for

538   all BTH2+26 cities in Fig. 9d show obvious improvement in PM$_{2.5}$ simulations after including CPM

539   emissions, with the NMB values from -36.5% in the base case to -14.1% in the S1.1 case, and then to 6.8%

540   in the S1.3 case. Nevertheless, there were still model-measurement biases for PM$_{2.5}$ concentrations in

541   some cities with high observations exceeding 90 µg m^{-3}, including Baoding, Anyang, Puyang, Heze,

542   Zhengzhou and Kaifeng. The insufficient improvement of PM$_{2.5}$ can be attributed to incomplete emission

543   information of inorganic components, which need further research. In addition, some heavy pollution

544   hours were chosen to investigate the regional impacts of CPM on PM$_{2.5}$ concentrations, including 8:00,

545   9:00, 10:00, 11:00, and 21:00 on December 15 (Fig. 10a). Besides the BTH2+26 cities, some surrounding

546   cities (Chaoyang, Chengde, Datong, Dongying, Huludao, Jinzhou, Linxi, Luoyang, Luohe, Qinhuangdao,

547   Qindao, Rizhao, Sanmenxia, Shangqiu, Shuozhou, Taian, Weihai, Weifang, Xinzhou, Xinyang, Yantai,

548   Zaozhuang, Zhangjiakou, Zhoukou, Zhunmadian) were also included. Results show that the

549   underestimated PM$_{2.5}$ concentrations in the base case were substantially improved after considering CPM

550   emissions in S1.1 and S1.3, especially for some high observations over 170 µg m^{-3}. Better agreement

551   between simulated and observed PM$_{2.5}$ concentrations for all these cities was achieved, with the NMB

552   values from -36.0% in the base case to -15.3% in S1.1, and to 3.3% in S1.3 (Fig. 10b). To sum up, the

553   consideration of CPM effects can improve the underestimation of regional OA and PM$_{2.5}$ simulations to

554   a certain extent, especially during the heavy pollution periods.

555

4 Conclusions

557   In this study, we focused on emissions of condensable PM from stationary combustion and mobile

558   sources and developed an emission inventory of organic CPM in China. Using emission inputs with and

559   without CPM contributions, the CMAQ model was applied to simulate the impacts of CPM on

560   atmospheric OA and PM$_{2.5}$ in China. The results show that the inclusion of CPM emissions increased

561   annual OA emissions by a factor of 2 for both the years 2014 and 2017. The power plant, industry

562   combustion, and steel sectors in the stationary combustion sources dominated OA emissions in the new

563   inventory. A series of sensitivity scenarios with different emission ratios and volatility distributions show

564   that CPM contributed significantly to the improvement of hourly SOA and POA concentrations during

565   the period from October 14 to November 14, 2014, at Beijing. The contributions of CPM were 53 ~ 86%

566   to POA and 48 ~ 67% to SOA under these scenarios. The model comparison against observations suggests

567   that the consideration of CPM effects improved the underestimations of simulation results and achieved

568   a good capture of peak SOA and POA values. In addition, the enhancements of daily OA levels by CPM

569   were demonstrated during December 6-30, 2018 at Handan, Shijiazhuang, Xingtai and Dezhou.

570   Compared to daily observations, the NMB values in these four cities were improved from -68%, -63%, -

571   75%, -71% (the base case) to -28%, -13%, -36%, -33% (the S1.1 case) for OA, respectively. The regional

572   contributions of CPM also narrowed the gap between simulated and observed concentrations of $PM_{2.5}$ in

573   the BTH2+26 cities. In conclusion, our estimated CPM emissions contributed significantly to the

574   improvements of simulation performances for both atmospheric OA and $PM_{2.5}$, especially during the high

575   pollution episodes. Therefore, the CPM emissions can be incorporated into chemical transport models

576   together with FPM to improve the simulation accuracies of OA and $PM_{2.5}$.

577   Our estimates of organic CPM emissions and SOA formation from CPM contained the following

578   uncertainties: (1) The construction of the organic CPM emission inventory in the present study was based

579   on the ratios of E_{POA}(CPM) to $E_{PM2.5}$(FPM) derived from limited sources, instead of the actual

580   measurement data of CPM emissions from the different sources and regions over China. (2) Since there

581   was no explicit volatility characterization of primary organic CPM species available for incorporation

582   into the emission inventories, the S/IVOCs emissions were scaled to the POA emissions. (3) Due to the

583   lack of relevant data, the original surrogate species of S/IVOCs and their properties in the CMAQ model

584   remained unchanged for representing the SOA formation from CPM, rather than introducing new model

585   species with identified parameters related to OH reaction rates, effective saturation concentration, and

586   multigenerational aging products. Based on these limitations, it is strongly recommended that future

587   studies conduct extensive surveys of CPM emissions from various stationary combustion sources and

588   measure the actual emissions of source-specific and region-specific S/IVOCs to better constrain OA

589   simulations by chemical transport models.

590

591   ***Data availability.*** The emission data and model results are available upon request.

Atmospheric
Chemistry
and Physics
Discussions

612   **References**

613   Ansari, T. U., Wild, O., Li, J., Yang, T., Xu, W., Sun, Y. and Wang, Z.: Effectiveness of short-term air quality emission
614   controls: a high-resolution model study of Beijing during the Asia-Pacific Economic Cooperation (APEC) summit
615   period, Atmos. Chem. Phys., 19(13), 8651–8668, doi:10.5194/acp-19-8651-2019, 2019.
616   Appel, K. W., Bash, J. O., Fahey, K. M., Foley, K. M., Gilliam, R. C., Hogrefe, C., Hutzell, W. T., Kang, D., Mathur, R.,
617   Murphy, B. N., Napelenok, S. L., Nolte, C. G., Pleim, J. E., Pouliot, G. A., Pye, H. O. T., Ran, L., Roselle, S. J.,
618   Sarwar, G., Schwede, D. B., Sidi, F. I., Spero, T. L. and Wong, D. C.: The Community Multiscale Air Quality (CMAQ)
619   model versions 5.3 and 5.3.1: System updates and evaluation, Geosci. Model Dev., 14(5), 2867–2897,
620   doi:10.5194/gmd-14-2867-2021, 2021.
621   Carlton, A. G. and Baker, K. R.: Photochemical modeling of the ozark isoprene volcano: MEGAN, BEIS, and their
622   impacts on air quality predictions, Environ. Sci. Technol., 45(10), 4438–4445, doi:10.1021/es200050x, 2011.
623   Carlton, A. G., Wiedinmyer, C. and Kroll, J. H.: A review of Secondary organic aerosol (SOA) formation from isoprene,
624   Atmos. Chem. Phys., 9(14), 4987–5005, doi:10.5194/acp-9-4987-2009, 2009.
625   Chen, L., Zhu, J., Liao, H., Gao, Y., Qiu, Y., Zhang, M., Liu, Z., Li, N. and Wang, Y.: Assessing the formation and
626   evolution mechanisms of severe haze pollution in the Beijing-Tianjin-Hebei region using process analysis, Atmos.
627   Chem. Phys., 19(16), 10845–10864, doi:10.5194/acp-19-10845-2019, 2019.

628 Choi, Y. J. and Fernando, H. J. S.: Implementation of a windblown dust parameterization into MODELS-3/CMAQ:
629   Application to episodic PM events in the US/Mexico border, Atmos. Environ., 42(24), 6039–6046,
630   doi:10.1016/j.atmosenv.2008.03.038, 2008.

631 Corio, L.A., Sherwell, J.: In-stack condensible particulate matter measurements and issues. J. Air Waste Manage. Assoc.
632   50, 207–218, 2000.

633 Donahue, N. M., Robinson, A. L., Stanier, C. O., and Pandis, S. N.: Coupled partitioning, dilution, and chemical aging of
634   semivolatile organics, Environ. Sci. Technol., 40, 2635–2643, https://doi.org/10.1021/es052297c, 2006.

635 Donahue, N. M., Epstein, S. A., Pandis, S. N., and Robinson, A. L.: A two-dimensional volatility basis set: 1. organic-
636   aerosol mixing thermodynamics, Atmos. Chem. Phys., 11, 3303–3318, https://doi.org/10.5194/acp-11-3303-2011, 2011.

637 Dong, Z., Wang, S., Xing, J., Chang, X., Ding, D. and Zheng, H.: Regional transport in Beijing-Tianjin-Hebei region and
638   its changes during 2014–2017: The impacts of meteorology and emission reduction, Sci. Total Environ., 737, 139792,
639   doi:10.1016/j.scitotenv.2020.139792, 2020.

640 Emery, C., Tai, E. and Yarwood, G.: Enhanced meteorological modeling and performance evaluation for two Texas ozone
641   episodes, Texas Natural Resource Conservation Commission, ENVIRON International Corporation, pp. 1–235.
642   Available online: http://www.tceq.state.tx.us/assets/public/implementation/air/am/contracts/reports/mm/
643   EnhancedMetModelingAndPerformanceEvaluation.pdf.

644 EPA, United States Environmental Protection Agency, Method 202 A – Dry Impinger Method for Determining
645   Condensable Particulate Emissions from Stationary Sources, 2017.

646 Feng, Y., Li, Y., Cui, L.: Critical review of condensable particulate matter, Fuel, 224, 801–813, 2018.

647 Feng, Y., Li, Y., Zhang, X., Su, S., Zhang, Z., Gan, Z. and Dong, Y.: Comparative study on the characteristics of
648   condensable particulate matter emitted from three kinds of coal, Environ. Pollut., 270, 116267,
649   doi:10.1016/j.envpol.2020.116267, 2021.

650 Fu, T. M., Cao, J. J., Zhang, X. Y., Lee, S. C., Zhang, Q., Han, Y. M., Qu, W. J., Han, Z., Zhang, R., Wang, Y. X., Chen,
651   D. and Henze, D. K.: Carbonaceous aerosols in China: Top-down constraints on primary sources and estimation of
652   secondary contribution, Atmos. Chem. Phys., 12(5), 2725–2746, doi:10.5194/acp-12-2725-2012, 2012.

653 Fuzzi, S., Andreae, M. O., Huebert, B. J., Kulmala, M., Bond, T. C., Boy, M., Doherty, S. J., Guenther, A., Kanakidou,
654   M., Kawamura, K., Kerminen, V. M., Lohmann, U., Russell, L. M. and Pöschl, U.: Critical assessment of the current
655   state of scientific knowledge, terminology, and research needs concerning the role of organic aerosols in the
656   atmosphere, climate, and global change, Atmos. Chem. Phys., 6(7), 2017–2038, doi:10.5194/acp-6-2017-2006, 2006.

657 Gao, M., Carmichael, G. R., Wang, Y., Saide, P. E., Yu, M., Xin, J., Liu, Z. and Wang, Z.: Modeling study of the 2010
658   regional haze event in the North China Plain, Atmos. Chem. Phys., 16(3), 1673–1691, doi:10.5194/acp-16-1673-2016,
659   2016.

660 Gehring, U., Gruzieva, O., Agius, R. M., Beelen, R., Custovic, A., Cyrys, J., Eeftens, M., Flexeder, C., Fuertes, E.,
661   Heinrich, J., Hoffmann, B., de Jongste, J. C., Kerkhof, M., Klümper, C., Korek, M., Mölter, A., Schultz, E. S., Simpson,
662   A., Sugiri, D., Svartengren, M., von Berg, A., Wijga, A. H., Pershagen, G. and Brunekreef, B.: Air pollution exposure
663   and lung function in children: The ESCAPE project, Environ. Health Perspect., 121(11–12), 1357–1364,
664   doi:10.1289/ehp.1306770, 2013.

665 Van Der Gon, H. A. C. D., Bergström, R., Fountoukis, C., Johansson, C., Pandis, S. N., Simpson, D. and Visschedijk, A. J.
666   H.: Particulate emissions from residential wood combustion in Europe - revised estimates and an evaluation, Atmos.
667   Chem. Phys., 15(11), 6503–6519, doi:10.5194/acp-15-6503-2015, 2015.

668 Grieshop, A. P., Logue, J. M., Donahue, N. M. and Robinson, A. L.: Laboratory investigation of photochemical oxidation
669   of organic aerosol from wood fires 1: measurement and simulation of organic aerosol evolution, Atmos. Chem. Phys.,
670   9, 1263–1277, 2009.

671 Han, Z., Xie, Z., Wang, G., Zhang, R. and Tao, J.: Modeling organic aerosols over east China using a volatility basis-set
672   approach with aging mechanism in a regional air quality model, Atmos. Environ., 124, 186–198,
673   doi:10.1016/j.atmosenv.2015.05.045, 2016.

674 Hayes, P. L., Carlton, A. G., Baker, K. R., Ahmadov, R., Washenfelder, R. A., Alvarez, S., Rappenglück, B., Gilman, J.

675   B., Kuster, W. C., De Gouw, J. A., Zotter, P., Prévôt, A. S. H., Szidat, S., Kleindienst, T. E., Offenberg, J. H., Ma, P. K.
676   and Jimenez, J. L.: Modeling the formation and aging of secondary organic aerosols in Los Angeles during CalNex
677   2010, Atmos. Chem. Phys., 15(10), 5773–5801, doi:10.5194/acp-15-5773-2015, 2015.

678 He, X., Wang, Q., Huang, X. H. H., Huang, D. D., Zhou, M., Qiao, L., Zhu, S., Ma, Y. ge, Wang, H. li, Li, L., Huang, C.,
679   Xu, W., Worsnop, D. R., Goldstein, A. H. and Yu, J. Z.: Hourly measurements of organic molecular markers in urban
680   Shanghai, China: Observation of enhanced formation of secondary organic aerosol during particulate matter episodic
681   periods, Atmos. Environ., 240, doi:10.1016/j.atmosenv.2020.117807, 2020.

682 Hu, Y., Feng, Y., Wang, C., Ma, Z. and Jiang, T.: Studies on Monitoring Method of Condensable Particulate and Water-
683   soluble Ions in Fumes from Coal Fired Boilers, Environ. Monit. Manag. Technol., 28(1), 41–45, 2016.

684 Huang, R. J., Zhang, Y., Bozzetti, C., Ho, K. F., Cao, J. J., Han, Y., Daellenbach, K. R., Slowik, J. G., Platt, S. M.,
685   Canonaco, F., Zotter, P., Wolf, R., Pieber, S. M., Bruns, E. A., Crippa, M., Ciarelli, G., Piazzalunga, A., Schwikowski,
686   M., Abbaszade, G., Schnelle-Kreis, J., Zimmermann, R., An, Z., Szidat, S., Baltensperger, U., El Haddad, I. and Prévôt,
687   A. S. H.: High secondary aerosol contribution to particulate pollution during haze events in China, Nature, 514(7521),
688   218–222, doi:10.1038/nature13774, 2015.

689 Huang, X., Ding, A., Gao, J., Zheng, B., Zhou, D., Qi, X., Tang, R., Wang, J., Ren, C., Nie, W., Chi, X., Xu, Z., Chen, L.,
690   Li, Y., Che, F., Pang, N., Wang, H., Tong, D., Qin, W., Cheng, W., Liu, W., Fu, Q., Liu, B., Chai, F., Davis, S. J.,
691   Zhang, Q. and He, K.: Enhanced secondary pollution offset reduction of primary emissions during COVID-19
692   lockdown in China, Natl. Sci. Rev., 8(2), doi:10.1093/nsr/nwaa137, 2021.

693 Jathar, S. H., Woody, M., Pye, H. O. T., Baker, K. R. and Robinson, A. L.: Chemical transport model simulations of
694   organic aerosol in southern California: Model evaluation and gasoline and diesel source contributions, Atmos. Chem.
695   Phys., 17(6), 4305–4318, doi:10.5194/acp-17-4305-2017, 2017.

696 Kanakidou, M., Seinfeld, J. H., Pandis, S. N., Barnes, I., Dentener, F. J., Facchini, M. C., Van Dingenen, R., Ervens, B.,
697   Nenes, A., Nielsen, C. J., Swietlicki, E., Putaud, J. P., Balkanski, Y., Fuzzi, S., Horth, J., Moortgat, G. K., Winterhalter,
698   R., Myhre, C. E. L., Tsigaridis, K., Vignati, E., Stephanou, E. G. and Wilson, J.: Organic aerosol and global climate
699   modelling: A review, Atmos. Chem. Phys., 5(4), 1053–1123, doi:10.5194/acp-5-1053-2005, 2005.

700 Kroll, J. H. and Seinfeld, J. H.: Chemistry of secondary organic aerosol: Formation and evolution of low-volatility
701   organics in the atmosphere, Atmos. Environ., 42(16), 3593–3624, doi:10.1016/j.atmosenv.2008.01.003, 2008.

702 Lane, T. E., Donahue, N. M. and Pandis, S. N.: Simulating secondary organic aerosol formation using the volatility basis-
703   set approach in a chemical transport model, Atmos. Environ., 42(32), 7439–7451, doi:10.1016/j.atmosenv.2008.06.026,
704   2008.

705 Li, P. F., Yan, R. C., Yu, S. C., Wang, S., Liu, W. P., and Bao, H. M.: Reinstate regional transport of PM2.5 as a major
706   cause of severe haze in Beijing, Proc Natl Acad Sci USA (PNAS), 112(21), E2739–E2740.
707   doi:10.1073/pnas.1502596112., 2015.

708 Li, H., Zhang, Q., Zhang, Q., Chen, C., Wang, L., Wei, Z., Zhou, S., Parworth, C., Zheng, B., Canonaco, F., Prévôt, A. S.
709   H., Chen, P., Zhang, H., Wallington, T. J. and He, K.: Wintertime aerosol chemistry and haze evolution in an extremely
710   polluted city of the North China Plain: Significant contribution from coal and biomass combustion, Atmos. Chem.
711   Phys., 17(7), 4751–4768, doi:10.5194/acp-17-4751-2017, 2017a.

712 Li, J., Zhang, M., Wu, F., Sun, Y. and Tang, G.: Assessment of the impacts of aromatic VOC emissions and yields of SOA
713   on SOA concentrations with the air quality model RAMS-CMAQ, Atmos. Environ., 158, 105–115,
714   doi:10.1016/j.atmosenv.2017.03.035, 2017b.

715 Li, J., Qi, Z., Li, M., Wu, D., Zhou, C., Lu, S., Yan, J. and Li, X.: Physical and Chemical Characteristics of Condensable
716   Particulate Matter from an Ultralow-Emission Coal-Fired Power Plant, Energy and Fuels, 31(2), 1778–1785,
717   doi:10.1021/acs.energyfuels.6b02919, 2017c.

718 Li, J., Li, X., Zhou, C., Li, M., Lu, S., Yan, J. and Qi, Z.: Study on the Influencing Factors of the Distribution
719   Characteristics of Polycyclic Aromatic Hydrocarbons in Condensable Particulate Matter, Energy and Fuels, 31(12),
720   13233–13238, doi:10.1021/acs.energyfuels.7b01991, 2017d.

721 Li, J.: Experimental study on emission characteristics of condensable particulate matter and typical organic pollutants in

coal-fired flue gas., Ph.D. thesis, School of Energy Engineering, Zhejiang University, China, 164 pp., 2018.

Li, X., Qiao, Y., Zhu, J., Shi, L. and Wang, Y.: The "APEC blue" endeavor: Causal effects of air pollution regulation on air quality in China, J. Clean. Prod., 168, 1381–1388, doi:10.1016/j.jclepro.2017.08.164, 2017e.

Li, Y., Ye, C., Liu, J., Zhu, Y., Wang, J., Tan, Z., Lin, W., Zeng, L. and Zhu, T.: Observation of regional air pollutant transport between the megacity Beijing and the North China Plain, Atmos. Chem. Phys., 16(22), 14265–14283, doi:10.5194/acp-16-14265-2016, 2016.

Li, X., Zhou, C., Li, J., Lu, S. and Yan, J.: Distribution and emission characteristics of filterable and condensable particulate matter before and after a low-low temperature electrostatic precipitator, Environ. Sci. Pollut. Res., 26(13), 12798–12806, doi:10.1007/s11356-019-04570-y, 2019.

Li, Y., Tan, Z., Ye, C., Wang, J., Wang, Y., Zhu, Y., Liang, P., Chen, X., Fang, Y., Han, Y., Wang, Q., He, D., Wang, Y. and Zhu, T.: Using wavelet transform to analyse on-road mobile measurements of air pollutants: A case study to evaluate vehicle emission control policies during the 2014 APEC summit, Atmos. Chem. Phys., 19(22), 13841–13857, doi:10.5194/acp-19-13841-2019, 2019.

Liang, P., Zhu, T., Fang, Y., Li, Y., Han, Y., Wu, Y., Hu, M. and Wang, J.: The role of meteorological conditions and pollution control strategies in reducing air pollution in Beijing during APEC 2014 and Victory Parade 2015, Atmos. Chem. Phys., 17(22), 13921–13940, doi:10.5194/acp-17-13921-2017, 2017.

Lin, C. Q., Liu, G., Lau, A. K. H., Li, Y., Li, C. C., Fung, J. C. H. and Lao, X. Q.: High-resolution satellite remote sensing of provincial $PM_{2.5}$ trends in China from 2001 to 2015, Atmos. Environ., 180, 110–116, doi:10.1016/j.atmosenv.2018.02.045, 2018.

Liu, Z., Gao, W., Yu, Y., Hu, B., Xin, J., Sun, Y., Wang, L., Wang, G., Bi, X., Zhang, G., Xu, H., Cong, Z., He, J., Xu, J., and Wang, Y.: Characteristics of $PM_{2.5}$ mass concentrations and chemical species in urban and background areas of china: Emerging results from the CARE-china network, Atmos. Chem. Phys., 18(12), 8849-8871, doi:10.5194/acp-18-8849-2018, 2018.

Lu, Q., Zhao, Y., and Robinson, A. L.: Comprehensive organic emission profiles for gasoline, diesel, and gas-turbine engines including intermediate and semi-volatile organic compound emissions, Atmos. Chem. Phys., 18(23), 17637-17654, doi:http://dx.doi.org/10.5194/acp-18-17637-2018, 2018.

Lu, C. M., Dat, N. D., Lien, C. K., Chi, K. H. and Chang, M. B.: Characteristics of Fine Particulate Matter and Polycyclic Aromatic Hydrocarbons Emitted from Coal Combustion Processes, Energy and Fuels, 33(10), 10247–10254, doi:10.1021/acs.energyfuels.9b02201, 2019.

Lu, Q., N. Murphy, B., Qin, M., J. Adams, P., Zhao, Y., O. T. Pye, H., Efstathiou, C., Allen, C. and L. Robinson, A.: Simulation of organic aerosol formation during the CalNex study: Updated mobile emissions and secondary organic aerosol parameterization for intermediate-volatility organic compounds, Atmos. Chem. Phys., 20(7), 4313–4332, doi:10.5194/acp-20-4313-2020, 2020.

Morino, Y., Chatani, S., Tanabe, K., Fujitani, Y., Morikawa, T., Takahashi, K., Sato, K. and Sugata, S.: Contributions of Condensable Particulate Matter to Atmospheric Organic Aerosol over Japan, Environ. Sci. Technol., 52(15), 8456–8466, doi:10.1021/acs.est.8b01285, 2018.

Murphy, B. N. and Pandis, S. N.: Simulating the formation of semivolatile primary and secondary organic aerosol in a regional chemical transport model, Environ. Sci. Technol., 43(13), 4722–4728, doi:10.1021/es803168a, 2009.

Murphy, B. N., Woody, M. C., Jimenez, J. L., Carlton, A. M. G., Hayes, P. L., Liu, S., Ng, N. L., Russell, L. M., Setyan, A., Xu, L., Young, J., Zaveri, R. A., Zhang, Q. and Pye, H. O. T.: Semivolatile POA and parameterized total combustion SOA in CMAQv5.2: Impacts on source strength and partitioning, Atmos. Chem. Phys., 17(18), 11107–11133, doi:10.5194/ACP-17-11107-2017, 2017.

Murphy, B. N., Nolte, C. G., Sidi, F., Bash, J. O., Appel, K. W., Jang, C., Kang, D., Kelly, J., Mathur, R., Napelenok, S., Pouliot, G. and Pye, H. O. T.: The detailed emissions scaling, isolation, and diagnostic (DESID) module in the Community Multiscale Air Quality (CMAQ) modeling system version 5.3.2, Geosci. Model Dev., 14(6), 3407–3420, doi:10.5194/gmd-14-3407-2021, 2021.

Odum, J. R., Hoffmann, T., Bowman, F., Collins, D., Flagan, R. C. and Seinfeld, J. H.: Gas/Particle Partitioning and

Atmospheric
Chemistry
and Physics
Discussions

769   Secondary Organic Aerosol Yields, Environ. Sci. Technol., 30, 2580–2585, doi:10.1021/ES950943+, 1996.

770 Pankow, J. F.: An absorption model of gas/particle partitioning of organic compounds in the atmosphere, Atmos. Environ.,
771   28(2), 185–188, doi:10.1016/1352-2310(94)90093-0, 1994.

772 Pei, B.: Determination and emission of condensable particulate matter from coal-fired power plants, Huanjing
773   Kexue/Environmental Sci., 36(5), 1544–1549, doi:10.13227/j.hjkx.2015.05.005, 2015.

774 Pennington, E., Seltzer, K., Murphy, B., Qin, M., Seinfeld, J. and Pye, H.: Modeling secondary organic aerosol formation
775   from volatile chemical products, Atmos. Chem. Phys., (July), 1–26, doi:10.5194/acp-2021-547, 2021.

776 Pope, C. A., Burnett, R. T., Thun, M. J., Calle, E. E., Krewski, D., Ito, K. and Thurston, G. D.: Lung cancer,
777   cardiopulmonary mortality, and long-term exposure to fine particulate air pollution, J. Am. Med. Assoc., 287(9), 1132–
778   1141, doi:10.1001/jama.287.9.1132, 2002.

779 Pye, H. O. T., Pinder, R. W., Piletic, I. R., Xie, Y., Capps, S. L., Lin, Y., Surratt, J. D., Zhang, Z., Gold, A., Luecken, D. J.,
780   Hutzell, W. T., Jaoui, M., Offenberg, J. H., Kleindienst, T. E., Lewandowski, M., and Edney, E. O.: Epoxide pathways
781   improve model predictions of isoprene markers and reveal key role of acidity in aerosol formation. Environmental
782   Science & Technology, 47(19), 11056-11064, https://doi.org/10.1021/es402106h, 2013.

783 Pye, H. O. T., Murphy, B. N., Xu, L., Ng, N. L., Carlton, A. G., Guo, H., Weber, R., Vasilakos, P., Appel, K. W.,
784   Budisulistiorini, S. H., Surratt, J. D., Nenes, A., Hu, W., Jimenez, J. L., Isaacman-VanWertz, G., Misztal, P. K., and
785   Goldstein, A. H.: On the implications of aerosol liquid water and phase separation for organic aerosol mass, Atmos.
786   Chem. Phys., 17, 343–369, https://doi.org/10.5194/acp-17-343-2017, 2017.

787 Qi, Z., Li, J., Wu, D., Xie, W., Li, X. and Liu, C.: Particulate Matter Emission Characteristics and Removal Efficiencies of
788   a Low-Low Temperature Electrostatic Precipitator, Energy and Fuels, 31(2), 1741–1746,
789   doi:10.1021/acs.energyfuels.6b02692, 2017.

790 Qin, M., Murphy, B. N., Isaacs, K. K., McDonald, B. C., Lu, Q., McKeen, S. A., Koval, L., Robinson, A. L., Efstathiou,
791   C., Allen, C. and Pye, H. O. T.: Criteria pollutant impacts of volatile chemical products informed by near-field
792   modelling, Nat. Sustain., 4(2), 129–137, doi:10.1038/s41893-020-00614-1, 2021.

793 Robinson, A. L., Donahue, N. M., Shrivastava, M. K., Weitkamp, E. A., Sage, A. M., Grieshop, A. P., Lane, T. E., Pierce,
794   J. R. and Pandis, S. N.: Rethinking organic aerosols: Semivolatile emissions and photochemical aging, Science (80-.).,
795   315(5816), 1259–1262, doi:10.1126/science.1133061, 2007.

796 Shrivastava, M., Fast, J., Easter, R., Gustafson, W. I., Zaveri, R. A., Jimenez, J. L., Saide, P. and Hodzic, A.: Modeling
797   organic aerosols in a megacity: Comparison of simple and complex representations of the volatility basis set approach,
798   Atmos. Chem. Phys., 11(13), 6639–6662, doi:10.5194/acp-11-6639-2011, 2011.

799 Shrivastava, M. K., Lane, T. E., Donahue, N. M., Pandis, S. N. and Robinson, A. L.: Effects of gas particle partitioning
800   and aging of primary emissions on urban and regional organic aerosol concentrations, J. Geophys. Res. Atmos.,
801   113(18), doi:10.1029/2007JD009735, 2008.

802 Simon, H., Bhave, P. V., Swall, J. L., Frank, N. H., and Malm, W. C.: Determining the spatial and seasonal variability in
803   OM/OC ratios across the US using multiple regression. Atmos. Chem. Phys., 11(6), 2933–2949,
804   https://doi.org/10.5194/acp-11-2933-2011, 2011.

805 Song, J., Lu, S., Wu, Y., Zhou, C., Li, X. and Li, J.: Migration and distribution characteristics of organic and inorganic
806   fractions in condensable particulate matter emitted from an ultralow emission coal-fired power plant, Chemosphere,
807   243, 125346, doi:10.1016/j.chemosphere.2019.125346, 2020.

808 Sun, Y., Du, W., Wang, Q., Zhang, Q., Chen, C., Chen, Y., Chen, Z., Fu, P., Wang, Z., Gao, Z. and Worsnop, D. R.: Real-
809   Time Characterization of Aerosol Particle Composition above the Urban Canopy in Beijing: Insights into the
810   Interactions between the Atmospheric Boundary Layer and Aerosol Chemistry, Environ. Sci. Technol., 49(19), 11340–
811   11347, doi:10.1021/acs.est.5b02373, 2015.

812 Tang, L., Qu, J. B., Mi, Z. F., Bo, X., Chang, X. Y., Anadon, L. D., Wang, S. Y., Xue, X. D., Li, S. B., Wang, X., and
813   Zhao, X. H.: Substantial emission reductions from Chinese power plants after the introduction of ultra-low emissions
814   standards, Nat. Energy, 4, 929–938, https://doi.org/10.1038/s41560-019-0468-1, 2019.

815 Veld, M. in t., Alastuey, A., Pandolfi, M., Amato, F., Pérez, N., Reche, C., Via, M., Minguillón, M. C., Escudero, M. and

816   Querol, X.: Compositional changes of PM2.5 in NE Spain during 2009–2018: A trend analysis of the chemical
817   composition and source apportionment, Sci. Total Environ., 795, doi:10.1016/j.scitotenv.2021.148728, 2021.
818   Wang, G., Deng, J., Ma, Z., Hao, J. and Jiang, J.: Characteristics of filterable and condensable particulate matter emitted
819   from two waste incineration power plants in China, Sci. Total Environ., 639, 695–704,
820   doi:10.1016/j.scitotenv.2018.05.105, 2018.
821   Wang, G., Deng, J., Zhang, Y., Li, Y., Ma, Z., Hao, J. and Jiang, J.: Evaluating Airborne Condensable Particulate Matter
822   Measurement Methods in Typical Stationary Sources in China, Environ. Sci. Technol., 54(3), 1363–1371,
823   doi:10.1021/acs.est.9b05282, 2020a.
824   Wang, K., Yang, L., Li, J., Sheng, Z., He, Q. and Wu, K.: Characteristics of condensable particulate matter before and
825   after wet flue gas desulfurization and wet electrostatic precipitator from ultra-low emission coal-fired power plants in
826   China, Fuel, 278(June), 118206, doi:10.1016/j.fuel.2020.118206, 2020b.
827   Wang, L. Q., Chen, X., Zhang, Y. B., Li, M. Y., Li, P. F., Jiang, L. H., Xia, Y., Li, Z., Li, J. L., Wang L., Hou, T. Y., Liu
828   W. P., Rosenfeld D., Zhu T., Zhang Y. H., Chen J. M., Wang S. X., Huang Y. L., Seinfeld, J. H., and Yu, S. C.:
829   Switching to electric vehicles can lead to significant reductions of PM2.5 and NO2 across China, One Earth, 4, 1037–
830   1048, https://doi.org/10.1016/j.oneear.2021.06.008, 2021.
831   Wang, L. Q., Li, M. Y., Yu, S. C., Chen, X., Li, Z., Zhang, Y. B., Jiang, L. H., Xia, Y., Li, J. L., Liu W. P., Li, P. F., Eric,
832   L., Rosenfeld, D., and Seinfeld, J. H.: Unexpected rises of ozone in urban and rural areas and sulfur dioxide in rural
833   areas during the coronavirus city lockdown in Hangzhou, China: Implications for air quality, Environ. Chem. Lett.,
834   18:1713–1723, doi: 10.1007/s10311-020-01028-3, 2020c.
835   Wu, B., Bai, X., Liu, W., Lin, S., Liu, S., Luo, L., Guo, Z., Zhao, S., Lv, Y., Zhu, C., Hao, Y., Liu, Y., Hao, J., Duan, L.
836   and Tian, H.: Non-Negligible Stack Emissions of Noncriteria Air Pollutants from Coal-Fired Power Plants in China:
837   Condensable Particulate Matter and Sulfur Trioxide, Environ. Sci. Technol., 54(11), 6540–6550,
838   doi:10.1021/acs.est.0c00297, 2020.
839   Wu, L., Wang, X., Lu, S., Shao, M. and Ling, Z.: Emission inventory of semi-volatile and intermediate-volatility organic
840   compounds and their effects on secondary organic aerosol over the Pearl River Delta region, Atmos. Chem. Phys.,
841   19(12), 8141–8161, doi:10.5194/acp-19-8141-2019, 2019.
842   Wu, Y., Wang, P., Yu, S., Wang, L., Li, P., Li, Z., Mehmood, K., Liu, W., Wu, J., Lichtfouse, E., Rosenfeld, D. and
843   Seinfeld, J. H.: Residential emissions predicted as a major source of fine particulate matter in winter over the Yangtze
844   River Delta, China, Environ. Chem. Lett., 16(3), 1117–1127, doi:10.1007/S10311-018-0735-6/TABLES/3, 2018.
845   Xu, L., Pye, H. O. T., He, J., Chen, Y., Murphy, B. N., and Ng, N. L.: Experimental and model estimates of the
846   contributions from biogenic monoterpenes and sesquiterpenes to secondary organic aerosol in the southeastern United
847   States, Atmos. Chem. Phys., 18, 12613–12637, https://doi.org/10.5194/acp-18-12613-2018, 2018.
848   Xu, W. Q., Sun, Y. L., Chen, C., Du, W., Han, T. T., Wang, Q. Q., Fu, P. Q., Wang, Z. F., Zhao, X. J., Zhou, L. B., Ji, D.
849   S., Wang, P. C. and Worsnop, D. R.: Aerosol composition, oxidation properties, and sources in Beijing: Results from
850   the 2014 Asia-Pacific Economic Cooperation summit study, Atmos. Chem. Phys., 15(23), 13681–13698,
851   doi:10.5194/acp-15-13681-2015, 2015.
852   Yang, F., Li, Z., Liu, H., Feng, P., Tan, H., Zhang, S. and Lu, X.: Emission characteristics of condensable particulate
853   matter and sulfur trioxide from coal-fired power plants, J. Energy Inst., 94, 146–156, doi:10.1016/j.joei.2020.12.003,
854   2021.
855   Yang, H. H., Kuei-Ting Lee, Hsieh, Y.-S., Luo, S.-W. and Li, M.-S.: Filterable and Condensable Fine Particulate
856   Emissions from Stationary Sources, Aerosol Air Qual. Res., 14, 2010–2016, doi:10.4209/aaqr.2014.08.0175, 2014.
857   Yang, H. H., Arafath, S. M., Lee, K. T., Hsieh, Y. S. and Han, Y. Te: Chemical characteristics of filterable and
858   condensable $PM_{2.5}$ emissions from industrial boilers with five different fuels, Fuel, 232(168), 415–422,
859   doi:10.1016/j.fuel.2018.05.080, 2018a.
860   Yang, H. H., Arafath, S. M., Wang, Y. F., Wu, J. Y., Lee, K. T. and Hsieh, Y. S.: Comparison of Coal- and Oil-Fired
861   Boilers through the Investigation of Filterable and Condensable PM2.5 Sample Analysis, Energy and Fuels, 32(3),
862   2993–3002, doi:10.1021/acs.energyfuels.7b03541, 2018b.

863 Yu, S., Mathur, R., Pleim, J., Wong, D., Gilliam, R., Alapaty, K., Zhao, C. and Liu, X.: Aerosol indirect effect on the grid-
864   scale clouds in the two-way coupled WRF-CMAQ: Model description, development, evaluation and regional analysis,
865   Atmos. Chem. Phys., 14(20), 11247–11285, doi:10.5194/acp-14-11247-2014, 2014.

866 Zhang, Y., Tang, L., Croteau, P. L., Favez, O., Sun, Y., Canagaratna, M. R., Wang, Z., Couvidat, F., Albinet, A., Zhang,
867   H., Sciare, J., Prévôt, A. S. H., Jayne, J. T. and Worsnop, D. R.: Field characterization of the PM2.5 Aerosol Chemical
868   Speciation Monitor: Insights into the composition, sources, and processes of fine particles in eastern China, Atmos.
869   Chem. Phys., 17(23), 14501–14517, doi:10.5194/acp-17-14501-2017, 2017.

870 Zhang, Y., Chen, X., Yu, S., Wang, L., Li, Z., Li, M., Liu, W., Li, P., Rosenfeld, D. and Seinfeld, J. H.: City-level air
871   quality improvement in the Beijing-Tianjin-Hebei region from 2016/17 to 2017/18 heating seasons: Attributions and
872   process analysis, Environ. Pollut., 274, 116523, doi:10.1016/j.envpol.2021.116523, 2021.

873 Zhao, B., Wang, S., Donahue, N. M., Jathar, S. H., Huang, X., Wu, W., Hao, J., and Robinson, A. L.: Quantifying the
874   effect of organic aerosol aging and intermediate-volatility emissions on regional-scale aerosol pollution in China, Sci.
875   Rep., 6, 28815, https://doi.org/10.1038/srep28815, 2016.

876 Zhao, B., Wu, W., Wang, S., Xing, J., Chang, X., Liou, K. N., Jiang, J. H., Gu, Y., Jang, C., Fu, J. S., Zhu, Y., Wang, J.,
877   Lin, Y. and Hao, J.: A modeling study of the nonlinear response of fine particles to air pollutant emissions in the
878   Beijing-Tianjin-Hebei region, Atmos. Chem. Phys., 17(19), 12031–12050, doi:10.5194/acp-17-12031-2017, 2017.

879 Zhao, Y., Nguyen, N. T., Presto, A. A., Hennigan, C. J., May, A. A. and Robinson, A. L.: Intermediate Volatility Organic
880   Compound Emissions from On-Road Diesel Vehicles: Chemical Composition, Emission Factors, and Estimated
881   Secondary Organic Aerosol Production, Environ. Sci. Technol., 49(19), 11516–11526, doi:10.1021/acs.est.5b02841,
882   2015.

883 Zheng, C., Hong, Y., Liu, S., Yang, Z., Chang, Q., Zhang, Y., and Gao, X.: Removal and emission characteristics of
884   condensable particulate matter in an ultralow emission power plant, Energy & Fuels, 32(10), 10586-10594,
885   https://doi.org/10.1021/acs.energyfuels.8b02464, 2018.

886 Zheng, H., Cai, S., Wang, S., Zhao, B., Chang, X. and Hao, J.: Development of a unit-based industrial emission inventory
887   in the Beijing-Tianjin-Hebei region and resulting improvement in air quality modeling, Atmos. Chem. Phys., 19(6),
888   3447–3462, doi:10.5194/acp-19-3447-2019, 2019.

889 Zhou, C.: Experimental study on emission and distribution characteristics of organic pollutants in condensable particulate
890   matter in coal-fired flue gas., Master thesis, School of Energy Engineering, Zhejiang University, China, 82 pp., 2019.

891
892
893
894
895
896
897
898
899
900
901
902
903
904
905
906
907
908

909 Table 1 List of the ratios of the emission rates of OA in condensable particulate matter (CPM)
910 (E_{OA}(CPM)) to those of $PM_{2.5}$ in filterable particulate matter (FPM) ($E_{PM2.5}$(FPM)) from stationary
911 combustion sources based on the collected references.
912

method	emission sources	number	E_{OA}(CPM)/ $E_{PM2.5}$(FPM)			references
			[Min, Max]	Mean ± SD	median	
cooling method (EPA 202)	coal-fired power plant	30	[0.01, 25.4]	6.87 ± 7.25	3.99	Li et al. (2017c, 2017d); Li (2018); Li et al. (2019); Lu et al. (2019); Pei (2015); Qi et al. (2017); Song et al. (2020); Wang et al. (2020b); Wu et al. (2020); Yang et al. (2014, 2018b); Yang et al.(2021); Zhou (2019)
	waste incineration power plant	2	[1.64, 4.95]	3.29 ± 1.65	3.29	Wang et al. (2018)
	industrial coal-fired boiler	6	[0.14, 1.03]	0.58 ± 0.34	0.50	Lu et al. (2019) Yang et al. (2014, 2018a, 2018b)
	heavy oil-fired boiler	4	[0.28, 2.49]	1.62 ± 0.88	1.85	Yang et al. (2018a, 2018b)
	wood-fired boiler	1		0.03		
	natural gas-fired boiler	1		6.67		Yang et al. (2018a)
	diesel-fired boiler	1		15.84		
	iron and steel plants	5	[0.32, 7.22]	3.35 ± 2.21	3.00	Yang et al. (2014, 2015)
	incinerator	1		0.12		Yang et al. (2014)
dilution method (ISO 25597)	iron and steel coking plant	1		0.416		Zhang et al. (2020)

913
914
915
916
917
918
919
920
921
922
923
924
925
926

927 Table 2 Probabilistic distributions with uncertainty ranges in the ratio of E_{POA}(CPM) to $E_{PM2.5}$(FPM) (95%
928 confidence interval). Para1 represents the mean for normal, and the mean of ln(x) for lognormal. Para2
929 represents the standard deviation for normal, and the standard deviation of ln(x) for lognormal. Mean
930 represents the mean for emission ratios of each source category derived from the statistical bootstrap
931 simulation.
932

Input parameters	Emission sources	Distribution type	Para1	Para2	Mean	Uncertainty ranges (95% confidence level)
E_{POA}(CPM) /$E_{PM2.5}$(FPM)	Power plant	lognormal	1.07	0.93	4.12	(3.10, 5.29)
	Industry combustion	lognormal	-0.47	1.43	1.38	(0.62, 2.44)
	Steel	normal	2.80	1.98	2.80	(0.92, 4.50)
Total						(-27%, 28%)

933
934
935
936
937
938
939
940
941
942
943
944
945
946
947
948
949
950
951
952
953
954
955
956
957
958
959
960
961
962
963
964
965

966 Table 3 Simulation case design. PP, IN, IR, and TR denote source sectors of power plant, industry
967 combustion, steel, and transportation, respectively. Three kinds of scaling factors for the five volatility
968 bins of organic CPM are tested: fac1 (0.09, 0.09, 0.14, 0.18, 0.5) (Grieshop et al., 2009), fac2 (0.40, 0.26,
969 0.40, 0.51, 1.43) (Shrivastava et al., 2011), and fac3 (0.245, 0.175, 0.27, 0.345, 0.965) which is the average
970 of fac1 and fac2.
971

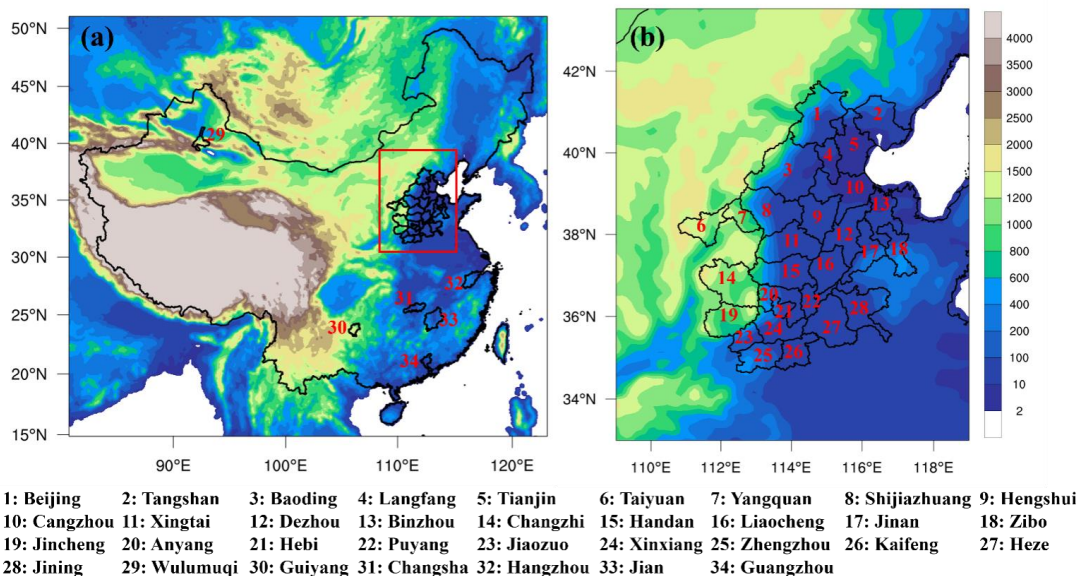| Simulation Cases	Aerosol module	E_{PP_POA}(CPM) /$E_{PM2.5}$(FPM)	E_{IN_POA}(CPM) /$E_{PM2.5}$(FPM)	E_{IR_POA}(CPM) /$E_{PM2.5}$(FPM)	Volatility bins
Only FPM	AERO6VBS	0	0	0	
	AERO7_def	0	0	0	
	AERO7_adj	0	0	0	
S1.1	AERO7	4.12	1.38	2.80	fac1
S1.2	AERO7	4.12	1.38	2.80	fac2
S1.3	AERO7	4.12	1.38	2.80	fac3
S2.1	AERO7	3.01	1.01	2.04	fac1
S2.2	AERO7	3.01	1.01	2.04	fac2
S3.1	AERO7	5.27	1.77	3.58	fac1
S3.2	AERO7	5.27	1.77	3.58	fac2
S4.2	AERO7	3.71	1.24	2.52	fac2
S5.2	AERO7	4.49	1.50	3.05	fac2
S6_TR	AERO7	0	0	0	fac1
S7_IN	AERO7	0	1.38	0	fac1
S8_IR	AERO7	0	0	2.80	fac1
S9_PP	AERO7	4.12	0	0	fac1

972
973
974
975
976
977
978
979
980
981
982
983
984
985
986
987
988
989
990
991
992
993

994 Table 4 Model evaluation statistics for hourly OA, POA and SOA concentrations during October 14–
995 November 14, 2014, and daily OA concentrations during December 6–30, 2018, under different
996 sensitivity simulation cases.

997

Period	City	Species	Cases	N	OBS	SIM	MB	NMB	NME	R
October 14– November 14, 2014	Beijing	OA	def		33.71	20.92	-12.79	-37.94%	50.06%	0.70
			adj		33.71	9.87	-23.84	-70.73%	70.80%	0.70
			S1.1	723	33.71	23.34	-10.37	-30.76%	48.03%	0.69
			S1.2		33.71	37.34	3.63	10.77%	56.28%	0.69
			S1.3		33.71	34.28	0.57	1.68%	53.45%	0.69
		POA	def		16.25	4.41	-11.84	-72.83%	72.94%	0.54
			adj		16.25	3.96	-12.29	-75.61%	75.66%	0.54
			S1.1	723	16.25	10.11	-6.14	-37.82%	54.14%	0.54
			S1.2		16.25	23.01	6.76	41.59%	85.95%	0.53
			S1.3		16.25	16.44	0.19	1.16%	60.87%	0.54
		SOA	def		17.46	16.50	-0.96	-5.47%	50.42%	0.73
			adj		17.46	5.90	-11.56	-66.19%	66.28%	0.73
			S1.1	723	17.46	13.23	-4.23	-24.20%	47.47%	0.72
			S1.2		17.46	14.33	-3.13	-17.90%	47.61%	0.72
			S1.3		17.46	17.84	0.38	2.16%	53.38%	0.72
December 6–30, 2018	Handan	OA	adj		45.24	14.66	-30.58	-67.58%	67.58%	0.62
			S1.1	25	45.24	32.37	-12.87	-28.45%	39.29%	0.60
			S1.3		45.24	49.69	4.45	9.84%	40.03%	0.59
	Shijiazhuang	OA	adj		42.22	15.57	-26.65	-63.12%	63.12%	0.61
			S1.1	25	42.22	36.70	-5.52	-13.07%	36.02%	0.61
			S1.3		42.22	59.07	16.85	39.90%	48.84%	0.61
	Xingtai	OA	adj		42.22	10.64	-31.58	-74.80%	74.80%	0.56
			S1.1	25	42.22	26.89	-15.33	-36.31%	44.14%	0.57
			S1.3		42.22	43.12	0.90	2.13%	34.85%	0.57
	Dezhou	OA	adj		41.66	12.07	-29.59	-71.02%	71.02%	0.48
			S1.1	23	41.66	28.10	-13.56	-32.55%	41.91%	0.55
			S1.3		41.66	42.98	1.32	3.17%	43.63%	0.57

998

999 Note: OBS and SIM denote mean concentrations (μg m^{-3}) of observations and simulations, respectively; MB: mean bias;
1000 NMB: normalized mean bias; NME: normalized mean error; R: correlation coefficient.

1: Beijing	2: Tangshan	3: Baoding	4: Langfang	5: Tianjin	6: Taiyuan	7: Yangquan	8: Shijiazhuang	9: Hengshui
10: Cangzhou	11: Xingtai	12: Dezhou	13: Binzhou	14: Changzhi	15: Handan	16: Liaocheng	17: Jinan	18: Zibo
19: Jincheng	20: Anyang	21: Hebi	22: Puyang	23: Jiaozuo	24: Xinxiang	25: Zhengzhou	26: Kaifeng	27: Heze
28: Jining	29: Wulumuqi	30: Guiyang	31: Changsha	32: Hangzhou	33: Jian	34: Guangzhou		

Figure 1. (a) Map of the modeling domain and location of each target city in model evaluation. (b) The locations of BTH2+26 cities, denoted as the red frame in (a).
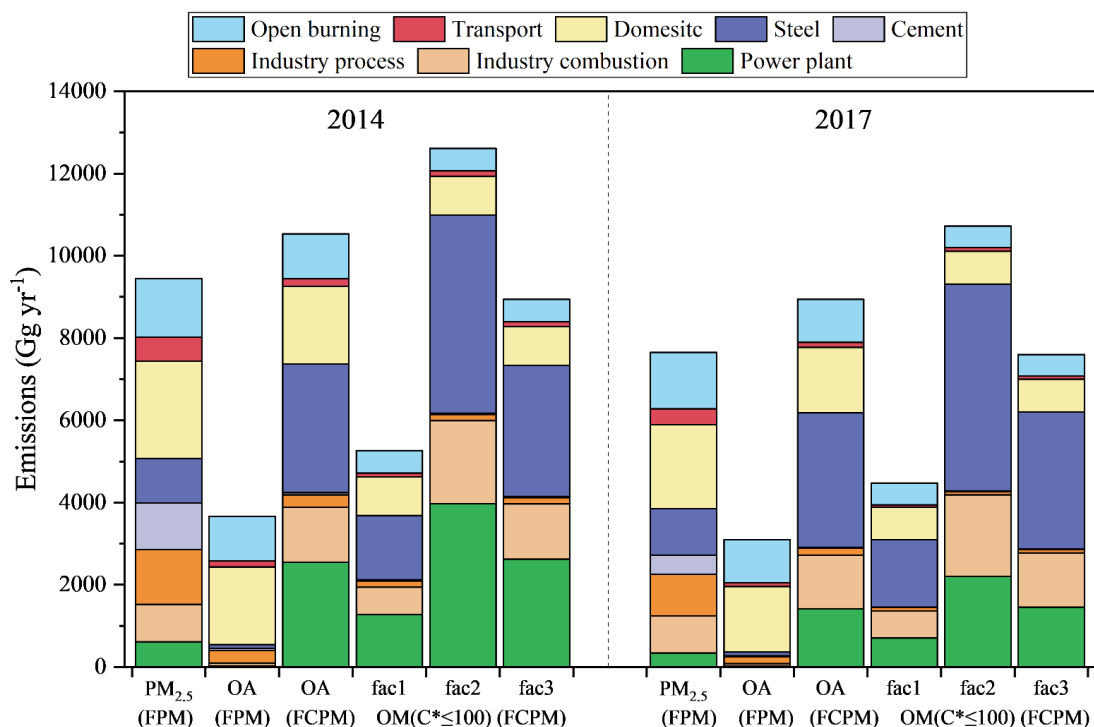
Figure 2. Annual emissions of $PM_{2.5}$ and OA in filterable particulate matter (FPM), OA in filterable plus condensable particulate matter (FCPM) before the volatility distributions, and OM ($C^* \leq 100$) in FCPM after application of the volatility distributions for the fac1, fac2 and fac3 cases over China in 2014 and 2017.
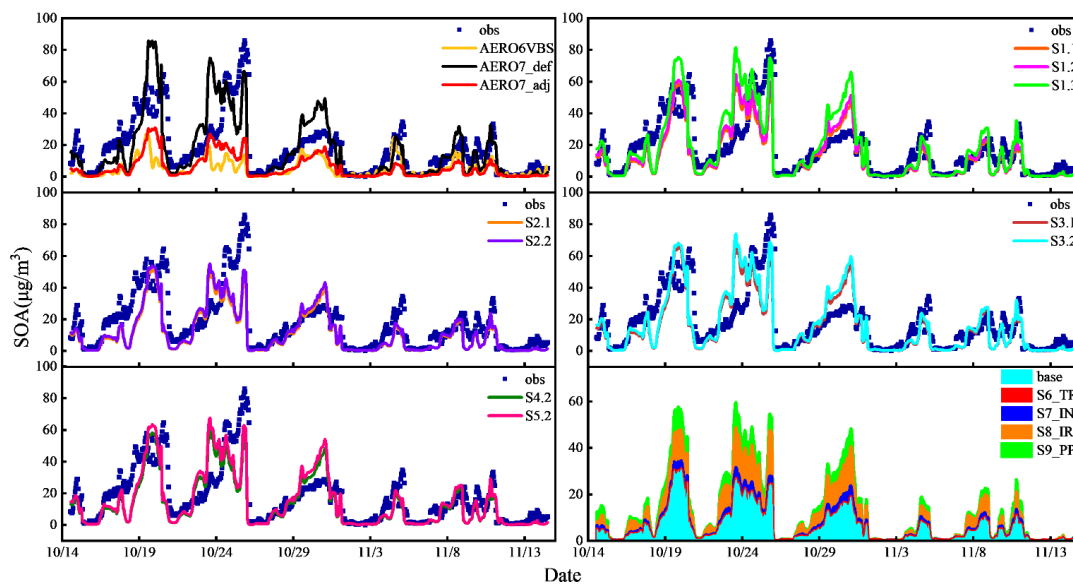
Figure 3. The observed and simulated hourly SOA concentrations during the episode from October 14 to November 14, 2014 at the Beijing site in the sensitivity cases as summarized in Table 3.
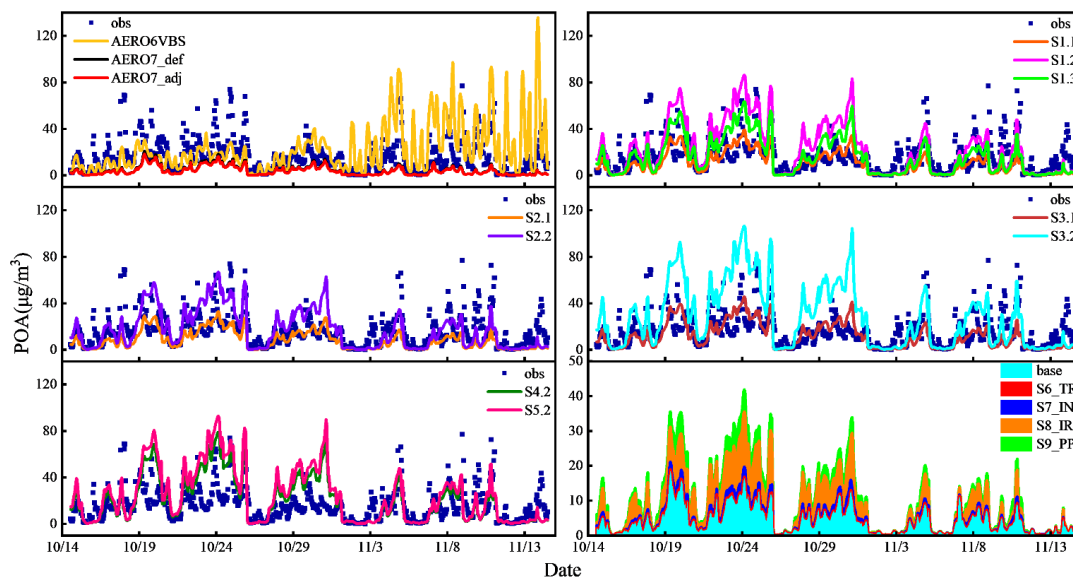
Figure 4. The observed and simulated hourly POA concentrations during the episode from October 14 to November 14, 2014 at the Beijing site in the sensitivity cases as summarized in Table 3.
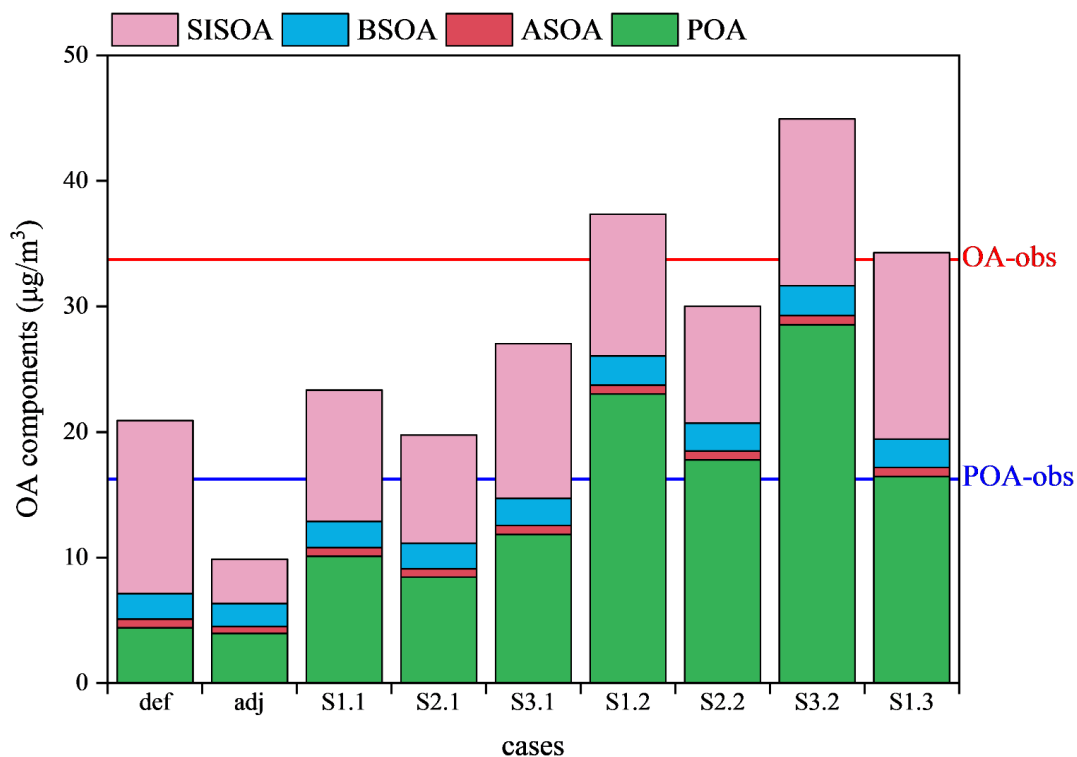
Figure 5. The simulation concentrations of different OA components averaged over the whole study period from October 14 to November 14, 2014 at the Beijing site in the sensitivity cases. AERO7_def is abbreviated as def and AERO7_adj as adj. ASOA, BSOA and SISOA denote SOA generated by anthropogenic VOCs, biogenic VOCs and low volatile S/IVOCs, respectively. The red and blue horizontal line denote the average observation concentrations of OA and POA, respectively.
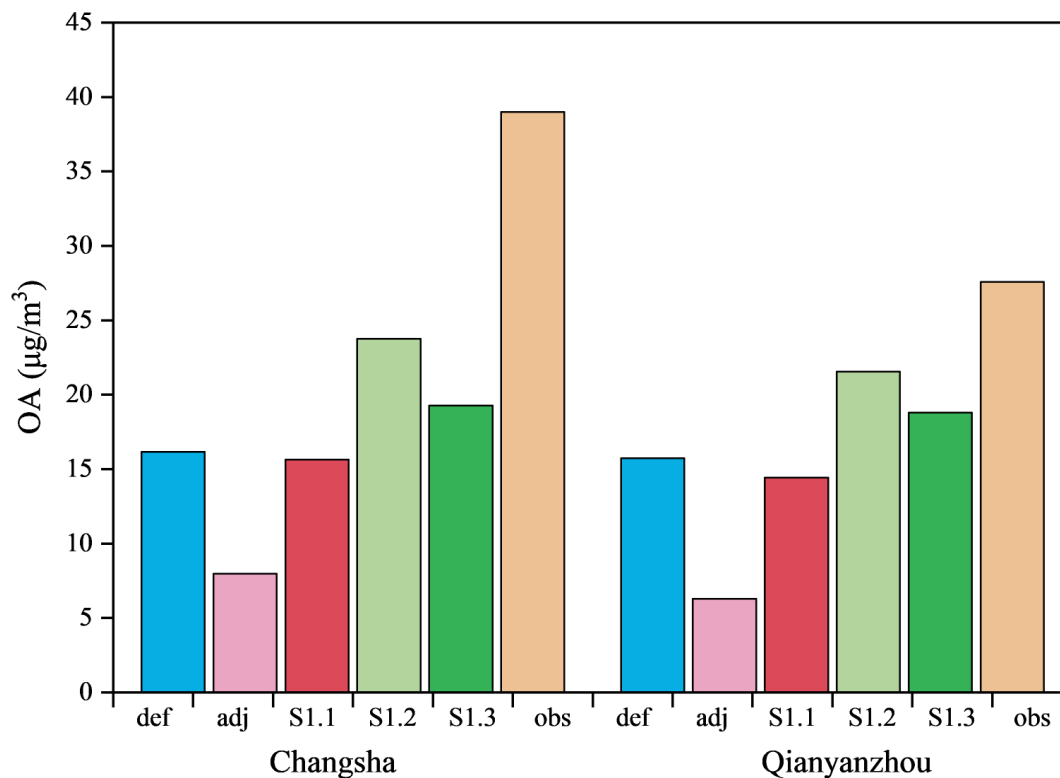
Figure 6. The observed and simulated OA concentrations in the sensitivity cases on November 3, 2014 at Changsha and Qianyanzhou.
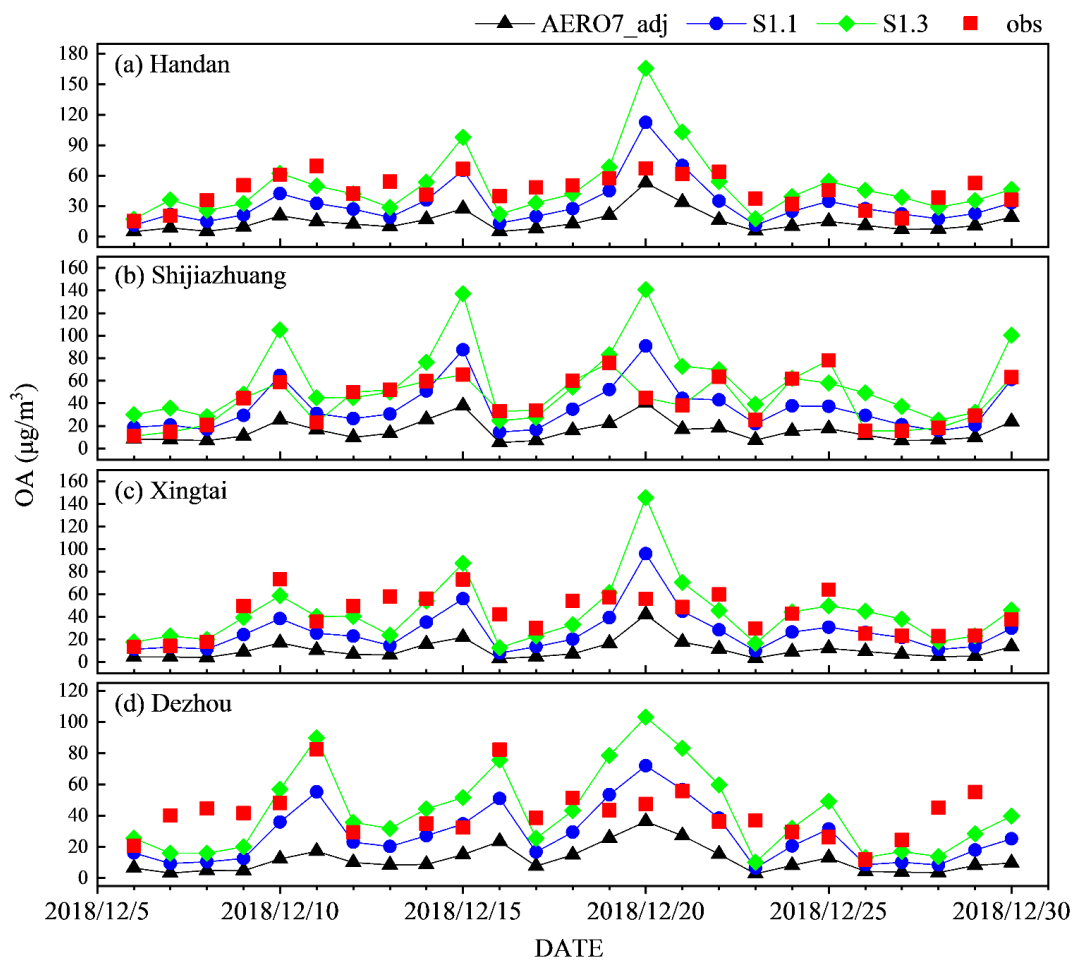
Figure 7. The observed and simulated daily OA concentrations during December 6-30 in 2018 at (a) Handan, (b) Shijiazhuang, (c) Xingtai and (d) Dezhou.
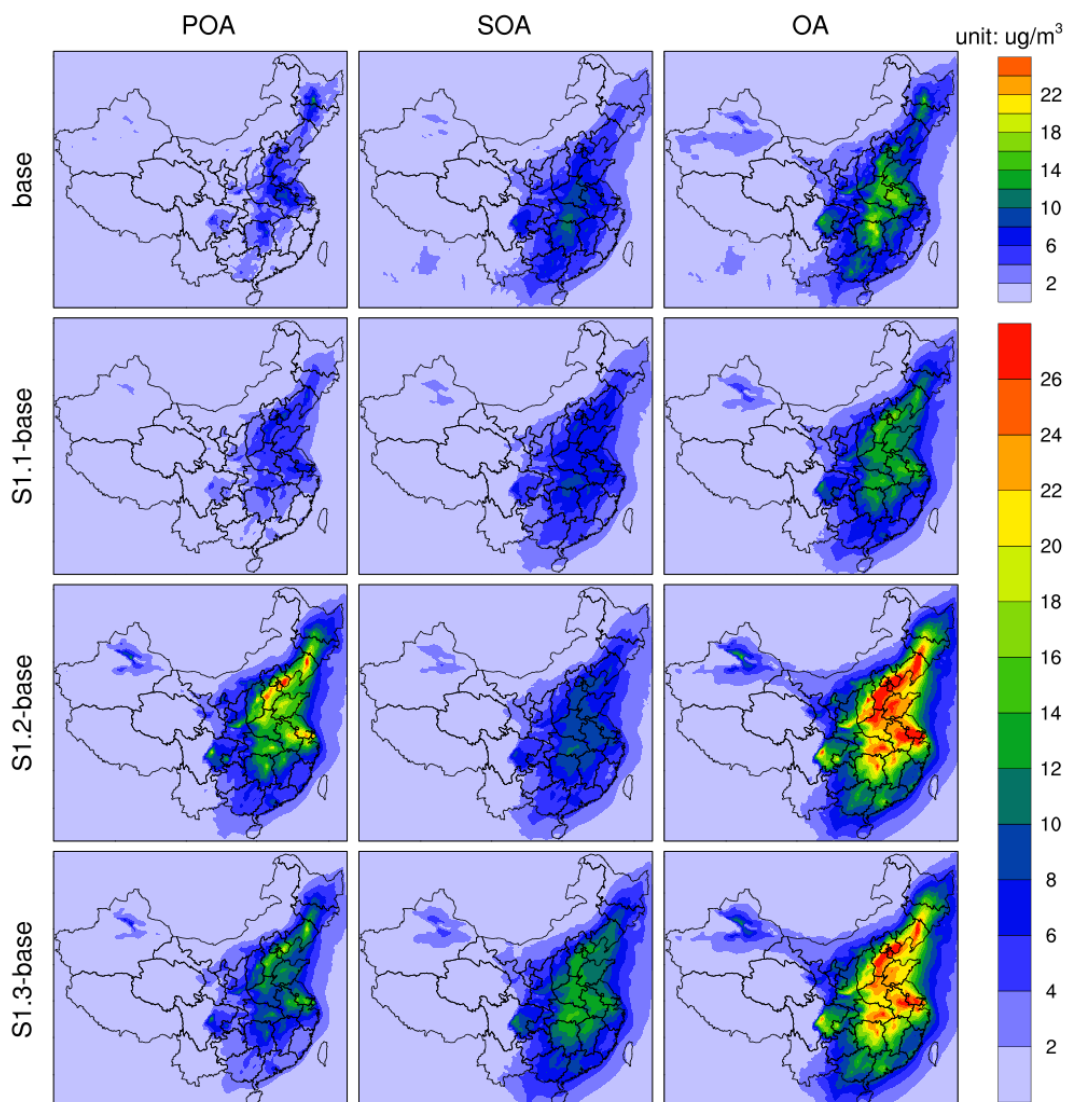
Figure 8. Spatial distributions of the concentrations of POA, SOA and OA averaged over the whole period of October 14-November 14 in 2014 generated by the simulations with FPM sources (base) and CPM sources (S1.1-base, S1.2-base, S1.3-base).
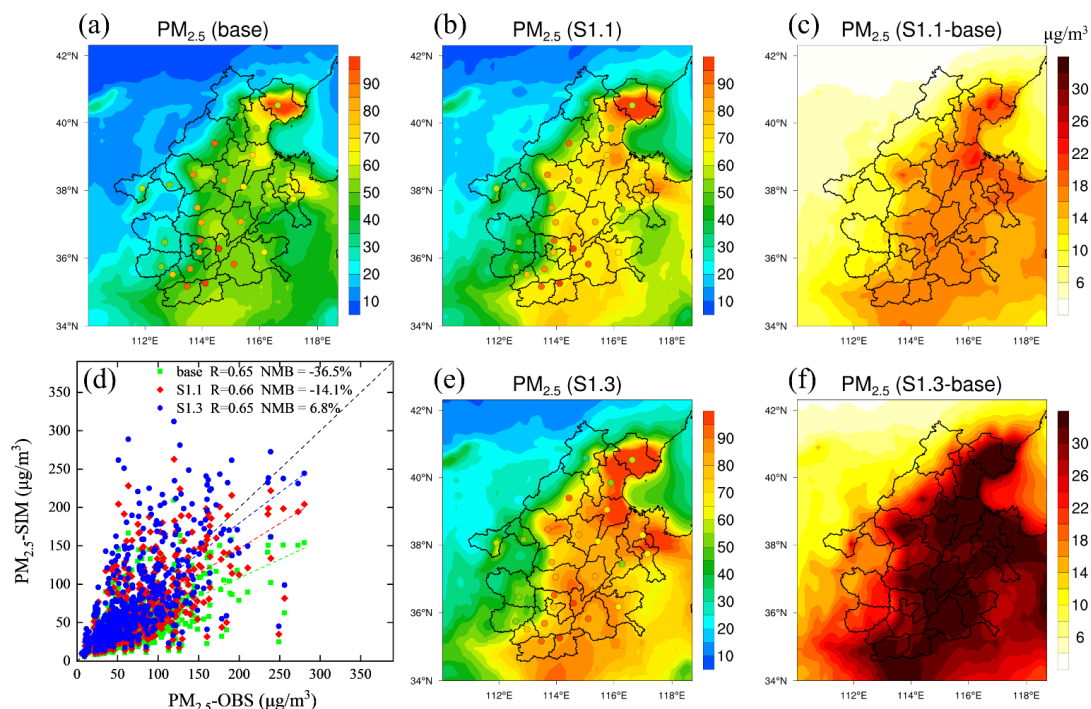
Figure 9. Spatial distributions of the average PM$_{2.5}$ concentrations during December 6-30, 2018, over the BTH2+26 cities in (a) base, (b) S1.1, (e) S1.3, (c) absolute difference between S1.1 and base, and (f) absolute difference between S1.3 and base. Among them, the PM$_{2.5}$ concentrations from December 22 to 26 are not included due to the missing observation data. (d) Scatter plots and linear regressions of observed (OBS) and simulated (SIM) daily PM$_{2.5}$ concentrations for all of the BTH2+26 cities during the above time period under the base, S1.1, and S1.3 scenarios.
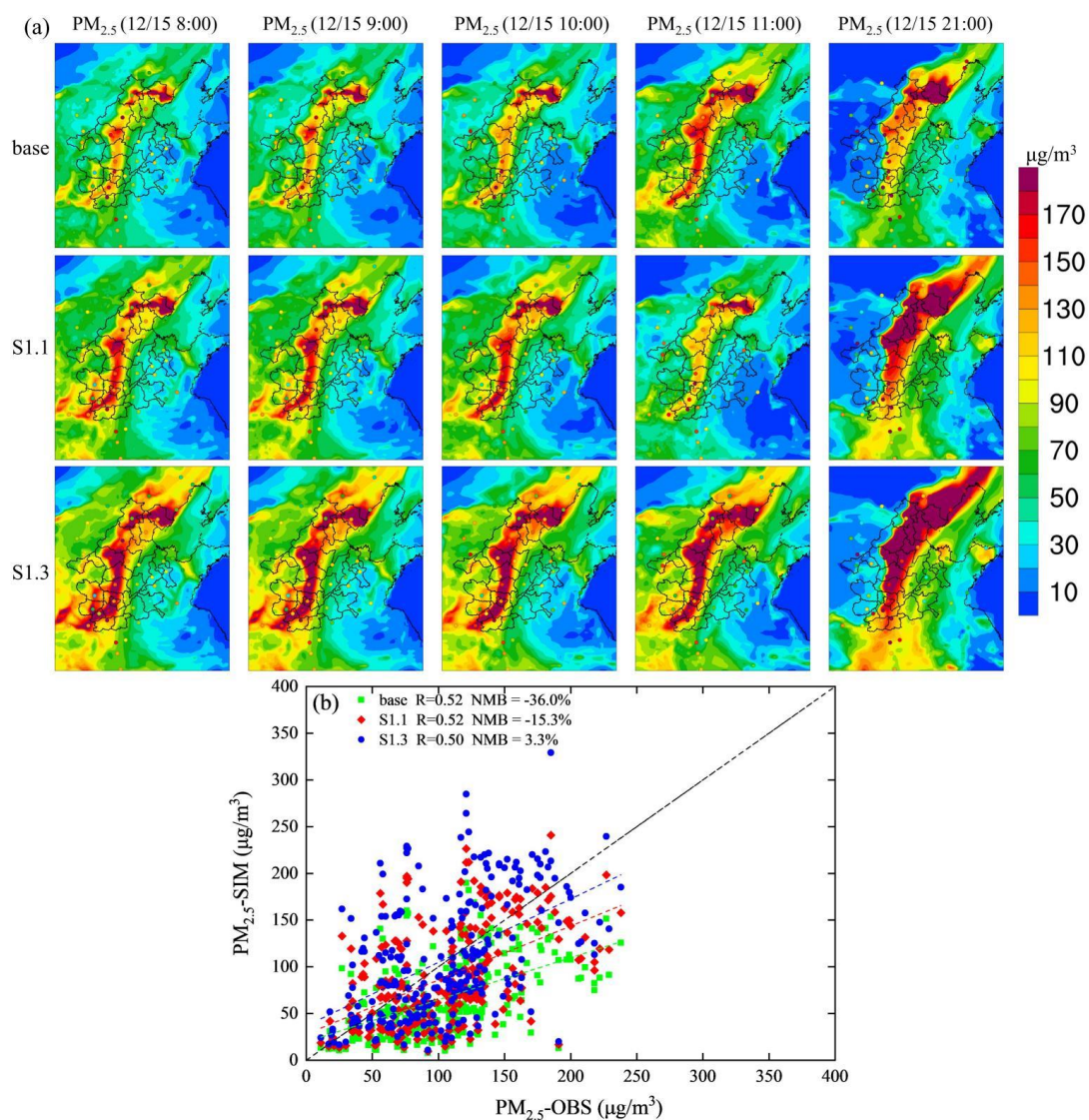
Figure 10. (a) Spatial distributions of hourly PM$_{2.5}$ concentrations at some peak hours over the BTH2+26 cities under the base, S1.1, and S1.3 scenarios. The colored dots denote observation values for each city. (b) Scatter plots and linear regressions of observed (OBS) and simulated (SIM) hourly PM$_{2.5}$ concentrations for all cities under the base, S1.1, and S1.3 scenarios.